Yang *et al. Microstructures* **2025**, *5*, 2025001
DOI: 10.20517/microstructures.2024.65

Microstructures

Review

Open Access

Check for updates

Preparation of Fe, Co, Ni-based single atom catalysts and the progress of their application in electrocatalysis

Yuquan Yang[1], Meifang Huang[1], Binbin Gao[2], Chenjing Wang[1], Hongjing Wu[1], Yanru Yuan[1], Jinlong Zheng[1,3]

[1]Beijing Advanced Innovation Center for Materials Genome Engineering, School of Mathematics and Physics, University of Science and Technology Beijing, Beijing 100083, China.
[2]North Institute for Scientific and Technical Information, Beijing 100089, China.
[3]Shunde Innovation School, University of Science and Technology Beijing, Foshan 528399, Guangdong, China.

Correspondence to: Dr. Jinlong Zheng, Beijing Advanced Innovation Center for Materials Genome Engineering, University of Science and Technology Beijing, No.30 Xueyuan Road, Haidian District, Beijing 100083, China. E-mail: zhengjinlong@ustb.edu.cn

How to cite this article: Yang, Y.; Huang, M.; Gao, B.; Wang, C.; Wu, H.; Yuan, Y.; Zheng, J. Preparation of Fe, Co, Ni-based single atom catalysts and the progress of their application in electrocatalysis. *Microstructures* **2025**, *5*, 2025001. https://dx.doi.org/10.20517/microstructures.2024.65

Received: 1 Aug 2024 **First Decision:** 9 Sep 2024 **Revised:** 23 Sep 2024 **Accepted:** 18 Oct 2024 **Published:** 11 Jan 2025

Academic Editors: Dingsheng Wang, Zhanxi Fan **Copy Editor:** Ping Zhang **Production Editor:** Ping Zhang

Abstract

Single-atom catalysts (SACs) have garnered considerable attention owing to their profound potential in promoting the efficient utilization of metal resources and attaining atomic-level economy. Fe, Co, Ni SACs have demonstrated broad application prospects in electrocatalysis due to their tunable composition and structure, as well as their unique electronic properties. Firstly, the various preparation methods for Fe, Co, Ni SACs are outlined in this review, including high-temperature pyrolysis, impregnation, chemical vapor deposition, and atomic layer deposition. These methods not only enhance the utilization efficiency of metal atoms but also ensure the stability of the catalysts. Subsequently, this review summarizes the recent progress in the applications of Fe, Co, Ni SACs for electrocatalysis, with a particular focus on their efficacy in hydrogen evolution reaction, oxygen evolution reaction, oxygen reduction reaction, carbon dioxide reduction reaction, and nitrogen reduction reaction. Despite remarkable advancements, Fe, Co, Ni SACs still face challenges related to large-scale production, stability enhancement, comprehensive characterization, and mechanistic exploration. Finally, this review discusses these challenges and proposes strategies to address them in order to fully realize the potential of Fe, Co, Ni SACs as high-performance catalysts.

Keywords: Single-atom catalyst, heterogeneous catalyst, atomic utilization rate, electrocatalysis, energy conversion

INTRODUCTION

Energy and electrocatalysis

Up to now, fossil fuels remain the primary energy source for industrial and agricultural production and human life. While they have driven unprecedented industrial development and wealth, they have also imposed unbearable environmental pressures on humanity. Moreover, fossil fuel reserves are limited, and long-term reliance on fossil fuels will lead to issues of energy supply shortages and environmental degradation. To solve energy scarcity and environmental pollution, the pursuit of eco-friendly, efficient and clean energy storage and conversion technologies has become increasingly crucial[1-3]. In this context, electrocatalytic technology has garnered significant attention due to its environmental friendliness and high efficiency. Catalysis plays a crucial role in the electrocatalytic process. Electrochemical catalysis is the use of an electric field to accelerate chemical reactions at the interface between an electrode and an electrolyte. The efficiency and selectivity of electrocatalytic reactions depend on the properties of the electrocatalyst. Different materials can all serve as electrocatalysts, and each material has its unique properties. For example, transition metal-based catalysts often exhibit high catalytic activity due to their ability to promote electron transfer. The surface structure and composition of electrocatalysts also play an important, decisive role in their performance. A well-designed electrocatalyst can increase the reaction rate and selectivity, thereby achieving more effective energy conversion. Common electrocatalytic reactions include oxygen reduction reaction (ORR)[4], oxygen evolution reaction (OER)[5], hydrogen evolution reaction (HER)[6], carbon dioxide reduction reaction (CO_2RR)[7], and nitrogen reduction reaction (NRR)[8]. In the electrocatalytic process, external electrons enter the reaction system through the electrode and interact with reactant molecules, altering their activation energy and thereby accelerating the rate of chemical reactions. By controlling parameters such as current and voltage, this technology enables precise regulation of reaction conditions, achieving effective control over chemical reactions.

Electrocatalysts

Electrocatalyst is a substance that can catalyze or accelerate the electrode reaction, and plays a key role in the electrocatalysis process. In electrocatalytic reactions, the electrocatalyst and the reactant are usually in different phase states, such as gas and solid, liquid and solid, *etc.*. Therefore, the reaction proceeds as a heterogeneous catalytic reaction, with the electrocatalyst functioning as a heterogeneous catalyst[9,10]. Heterogeneous catalysts are non-uniform nanoparticles or nanoparticles dispersed on solid support, which makes them easy to separate from the reaction system. However, due to the decrease in the dispersion of the active site, the reaction activity is inferior to that of homogeneous catalysts (which have maximum atom utilization efficiency, clear catalytic center and coordination structure). Additionally, due to the heterogeneity of particle size, side reactions will occur and the selectivity of reaction will be reduced[11,12]. Since the catalytic reaction occurs on the catalyst surface, increasing the surface atomic ratio of the active metal is conducive to promoting full contact between the reactants and the catalyst, which is the main solution to improve the catalyst reaction activity. As shown in Figure 1, as the size of nanoparticles gradually decreases from block to nanocluster and finally to single metal atom, the surface atom ratio of nanoparticles increases significantly, and the unsaturated coordination environment of metal species gradually increases, thus significantly improving the utilization efficiency of catalysts and ultimately leading to a substantial increase in catalytic activity[13-15]. Nevertheless, due to the uneven aggregation of metal atoms, the atomic utilization rate of heterogeneous catalysts is much lower than that of homogeneous catalysts (atomic utilization rate can reach 100%)[16]. Therefore, it is essential to control the heterogeneous catalyst at the atomic level to ensure the availability of abundant active sites. When the catalyst reaches the limit of single-atom size, 100% atom utilization can be achieved, thereby endowing it with high activity, enhanced selectivity and stable structure similar to that of the homogeneous catalyst, along with the easy separation characteristic of a heterogeneous catalyst[17-19].

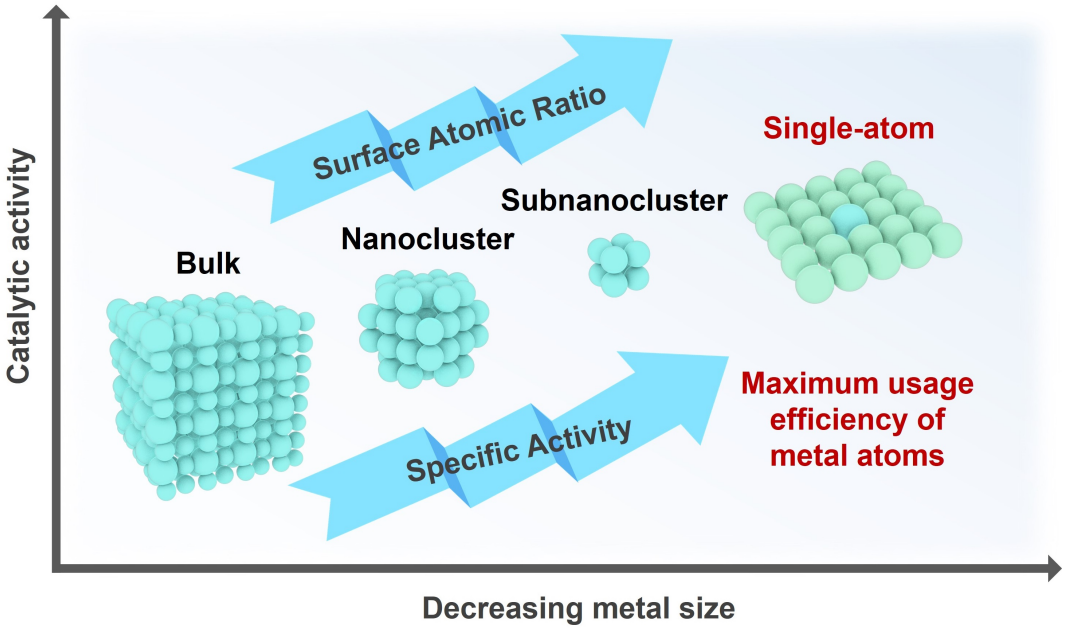

Figure 1. Schematic of the relationship between catalyst size, surface atomic ratio and catalytic activity. By decreasing the size of catalysts, the catalytic activity and selectivity will be improved substantially.

Single-atom catalysts

As a novel material, single-atom catalysts (SACs) have emerged as a groundbreaking frontier in the realm of heterogeneous catalysis owing to their exceptional atomic utilization and distinctive catalytic properties, offering greater prospects for the application of heterogeneous catalysis[20-22]. In 2011, researchers first introduced the concept of SACs, and the Pt_1/FeO_x catalyst (anchoring individual Pt atoms on the surface of FeO_x nanocrystals) they prepared exhibited good activity and stability for CO oxidation reactions. SACs represent an innovative class of catalysts characterized by the anchoring individual metal atoms in a highly dispersed form on the surface or inside the support material, forming a stable metal-support interaction[16,23]. Compared with traditional metal nanoparticle catalysts, SACs have the following significant characteristics: (i) Extremely high atomic utilization: since metal atoms exist in the form of individual atoms, the agglomeration of metal atoms is avoided, thereby greatly improving the utilization of metal atoms; (ii) Unique electronic structure: the presence of individual metal atoms changes their original electronic structure, making SACs exhibit different catalytic properties from traditional catalysts; (iii) Clear active sites: each metal atom in SACs is an independent active site, which helps to gain an in-depth understanding of the catalytic reaction mechanism[24,25]. At present, researchers have developed a series of single atomic catalysts, including platinum[4], palladium[26], iridium[27], gold[28], iron[18], cobalt[29], nickel[30], copper[31] and other single atomic sites, which are dispersed on metal oxides[32], hydrotalcite[13], carbon[33] and other supports. The SACs of iron, cobalt and nickel (Fe, Co, Ni SACs), which belong to the same iron group, have the following advantages and have received more attention[34-36]: (i) Abundant reserves on the earth: Fe, Co and Ni are relatively abundant elements on the earth with low cost and are conducive to large-scale industrial applications; (ii) Excellent catalytic performance: Fe, Co, Ni SACs show excellent activity, selectivity and stability in a variety of electrocatalytic reactions; (iii) Tunable electronic structure: By regulating the type, structure and coordination environment of the carrier and metal atoms, the electronic structure of Fe, Co and Ni SACs can be flexibly adjusted to optimize their catalytic performance.

Herein, we summarized the preparation methods of Fe, Co, Ni SACs, including high-temperature pyrolysis, impregnation, vapor deposition, atomic layer deposition (ALD), *etc.*. Subsequently, we review the great potential of Fe, Co, Ni SACs for clean energy conversion, including HER, OER, ORR, CO_2RR, NRR, *etc.*. Finally, the development and challenges of Fe, Co, Ni SACs are prospected from the aspects of preparation, characterization, catalytic mechanism, and industrial application. Furthermore, compared with other studies, this article has the following unique features. First, it focuses on iron, cobalt, and nickel-based SACs. On the basis of covering traditional preparation methods, it deeply discusses the application of new technologies such as chemical vapor deposition (CVD) and ALD in this field, including their principles, advantages, and challenges, thus providing readers with a more comprehensive and in-depth understanding. Secondly, it conducts in-depth research on the performance of these catalysts and reveals their catalytic mechanisms in different reactions. Furthermore, it extensively discusses the development trends of iron, cobalt, and nickel-based SACs. Finally, it introduces new viewpoints, research directions, and improvement ideas for addressing preparation problems. In short, in terms of focus, depth, breadth, and innovation, this article is significantly different from other related literature and is expected to make unique contributions to the research in this field.

PREPARATION METHODS OF FE, CO, NI SACS

A central challenge in the preparation of metal SACs is to ensure that the tiny metal active centers remain isolated and highly dispersed in complex chemical environments, avoiding migration and agglomeration[37]. The breakthrough point in this problem is to strengthen the bonding ability between the metal atoms and the catalyst supports, ensuring that they are closely linked[38,39]. To achieve this goal, researchers are dedicated to optimizing the selection of metal precursors and the design of catalyst supports, particularly focusing on the anchoring sites on the support surface. The objective is to stabilize the position of metal atoms by meticulously regulating the interactions between these elements[40,41]. Additionally, the precise control of the preparation process is also regarded as a crucial link, which directly affects the stability and efficiency of the single atom dispersion state in the final catalyst.

At present, researchers have adopted a variety of strategies to prepare Fe, Co, Ni SACs. The core idea of these strategies is to enhance the interaction between the metal and the support, so that the metal atoms or tiny clusters are firmly anchored to the surface of the support[42,43]. In addition, in order to promote the SAC from the laboratory to large-scale industrial applications, simplifying the operation process, lowering the technical threshold, and improving production efficiency has become another important research direction, aiming to achieve both efficient and economical production methods. Here, the preparation methods of Fe, Co, Ni SACs are mainly introduced: high-temperature pyrolysis, impregnation, CVD, ALD and other methods.

High-temperature pyrolysis

High-temperature pyrolysis has been extensively employed as a reliable technique for achieving the efficient dispersion of metal atoms. Most carbon-based electrocatalysts containing single metal sites are synthesized through this method[13]. This method utilizes the porous structures and high specific surface areas of various precursors, such as metal complexes[44], polymers[45], and metal-organic frameworks (MOFs)[46,47], to uniformly disperse metal atoms on the support during high-temperature treatment under an atmosphere (e.g., Ar, N_2, NH_3)[48-50]. During this process, the decomposition of metal-organic ligands fosters the establishment of robust bonds between the metal atoms and the support material, ultimately leading to the successful synthesis of SACs. High-temperature pyrolysis offers advantages including a straightforward preparation process and precise control over the catalyst structure. Nonetheless, it can also cause potential drawbacks such as support structure degradation and metal atom agglomeration, often necessitating the

additional step of acid etching to eliminate these aggregated metal particles.

Employing a high-temperature pyrolysis approach, Wei *et al.*[51] introduced a versatile "polymerization-coordination-pyrolysis" strategy for crafting SACs. This method has universal applicability. Three types of metal single atomic site catalysts are successfully prepared, namely Fe-isolated single-atom sites (ISASs)/CN, Co-ISASs/CN, and Ni-ISASs/CN. As shown in Figure 2A, firstly, a carbon sphere, based on porphyrin structure, was directly synthesized through the polymerization process involving terephthalaldehyde and pyrrole, two cost-effective small organic molecules that offer notable advantages over commercial metal-porphyrins monomers. Subsequently, by means of the formation of coordination bonds between nitrogen atoms (inherently present within the porphyrin structure) and metal ions, the porphyrin-based carbon sphere was strategically enriched with Fe, Co, or Ni ions. Finally, a series of Fe, Co, and Ni-ISASs/CN catalysts have been obtained by further pyrolysis via effective anchoring of Fe, Co, and Ni ISASs on the carbon nitride (CN) matrix. The energy dispersive X-ray spectroscopy (EDX) elemental mapping assessments verified a homogeneous dispersion of carbon, nitrogen, and metallic elements (Fe, Co, Ni) across the substrates [Figure 2B-D]. The direct visualization of isolated Fe, Co, and Ni single atoms (SAs) was presented as the bright dots highlighted with white circles in Figure 2E-G through aberration-corrected high-angle annular dark field scanning transmission electron microscopy (AC HAADF-STEM), signifying the presence of individual ISASs.

High-temperature pyrolysis is also widely employed in the preparation of SACs with MOF precursors. The main steps of synthesis involve crafting an appropriate MOF, subsequent pyrolysis treatment, and final acid etching. Notably, MOFs encompassed in this approach primarily consist of zeolitic imidazolate frameworks (ZIFs), metal polymers, and metal-organic compound molecules, showing the versatility of this methodology[33]. Wang *et al.*[52] prepared single-atom (SA)-Fe^{III}/sulfur and nitrogen co-doped porous carbon (SNPC) by high-temperature pyrolysis using zinc-based ZIFs (ZIF-8). During the pyrolysis process, sulfur was introduced and Zn was evaporated [Figure 2H]. The scanning electron microscopy (SEM) image [Figure 2I] and transmission electron microscopy (TEM) image [Figure 2J] reveal that no obvious Fe metal particles appear in SA-Fe^{III}/SNPC. The high-resolution AC HAADF-STEM image further confirms the atomic-scale dispersion of Fe [Figure 2K]. As shown in Figure 2L, the Fe K-edge X-ray absorption near edge structure (XANES) spectrum indicates that the Fe^{III}/SNPC exhibits higher energy owing to the formation of N-S bond in the second shell around Fe atoms. The Fourier transform of extended X-ray absorption fine structure (FT-EXAFS) spectrum [Figure 2M] shows the absence of Fe-Fe scattering path of Fe^{III}/SNPC, implying the atomically dispersed form of Fe atoms. The above results indicate that through the MOF-derived methodology, metal atoms can be effectively dispersed throughout the internal framework of carbon materials, resulting in the successful synthesis of metal SACs.

In addition to heat treatment at high temperatures, microwave heating can also be used to prepare SACs. For example, utilizing L-cysteine as an additional organic precursor in the polymerization process, an anchoring carbon platform (ACP) sheath is formed around a hybrid support consisting of carbon nanotubes (CNTs) and graphene (GR), characterized by small domain sizes, abundant edge sites, and sulfur doping. Single-atom M-N (M=Fe, Co, Ni, *etc.*) units are attached firmly on the ACP surface by a brief microwave pyrolysis step, which efficiently avoids the atom aggregation because of the obtained high graphitization of ACP during the high-temperature synthesis phase[53].

Impregnation

The impregnation method is a simple and commonly used technique for preparing SACs. This strategy refers to immersing the support material within a solution that contains metal precursors, followed by

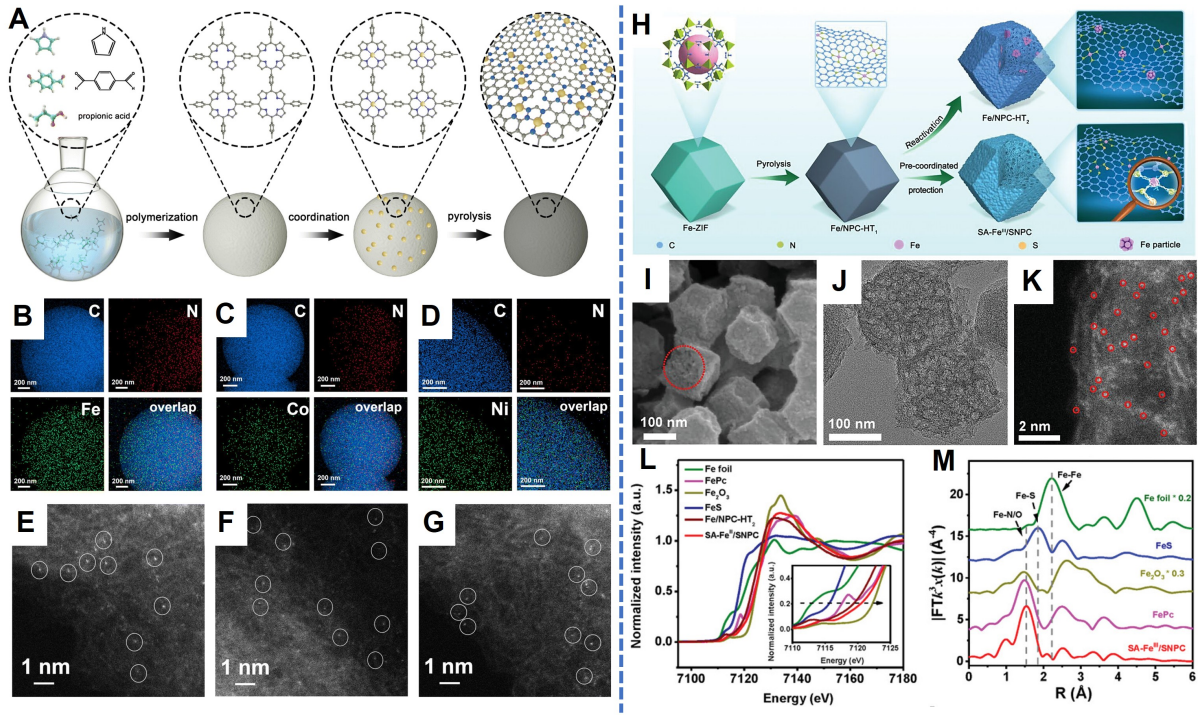

Figure 2. (A) Schematic illustration of the synthetic procedure of metal-ISASs/CN; (B-D) EDX measurements and (E-G) High-resolution AC HAADF-STEM images of Fe-ISASs/CN, Co-ISASs/CN and Ni-ISASs/CN, respectively. The (A-G) are quoted with permission from Wei *et al.*[51]; (H) Schematic illustration of preparation procedure for SA-Fe^{III}/SNPC catalyst; (I-K) SEM, TEM, and HAADF-STEM of SA-Fe^{III}/SNPC catalyst; (L) Fe XANES spectra and (M) Fe FT-EXAFS signal of SA-Fe^{III}/SNPC and reference samples. The (H-M) are quoted with permission from Zheng *et al.*[33]. XANES: X-ray absorption near edge structure; FT-EXAFS: Fourier transform of extended X-ray absorption fine structure; EDX: Energy-dispersive X-ray; AC HAADF-STEM: Aberration-corrected high-angle annular dark field scanning transmission electron microscopy; SNPC: Sulfur and nitrogen co-doped porous carbon; SEM: Scanning electron microscopy; TEM: Transmission electron microscopy; SAs: Single atoms; CN: Carbon nitride; ISAs: Isolated single-atom sites.

drying and heat treatment to anchor the metal atoms onto the support[54,55]. The key of impregnation method is to control the concentration of metal precursor, impregnation time and heat treatment temperature to prevent the agglomeration of metal atoms. While the impregnation process is relatively straightforward, easy to operate, and cost-effective, making it suitable for a variety of support and metal precursor combinations, it is not feasible for preparing high-metal-loading SACs. Furthermore, the dispersion of metal single atoms on the support surface is a complex process influenced by multiple intricate factors, making precise control challenging.

SACs obtained only through the impregnation process represent the most direct preparation method. The ion exchange or coordination between metal atoms and support during impregnation process induces the dispersion of single atoms on the support. For example, Yu *et al.*[13] loaded Fe SAs on the surface of amorphous Al_2O_3 by stirring at room temperature. Fourier Transform Infrared Spectroscopy (FTIR) analysis showed that the coordination between the Fe atoms and abundant OH groups on the surface of Al_2O_3 support was beneficial to the formation of isolated Fe SAs. Shi *et al.*[55] loaded Fe SAs onto organic polyaniline (PANI) through Fe-N coordination in the pyrolysis-free impregnation process, which significantly reduced the energy consumption in the catalyst preparation process [Figure 3A]. An AC HAADF-STEM image shows high-density iron atoms scattered on the surface of PANI [Figure 3B]. FT-EXAFS spectra presented in Figure 3C definitively confirm that the Fe atoms are primarily coordinated with N atoms.

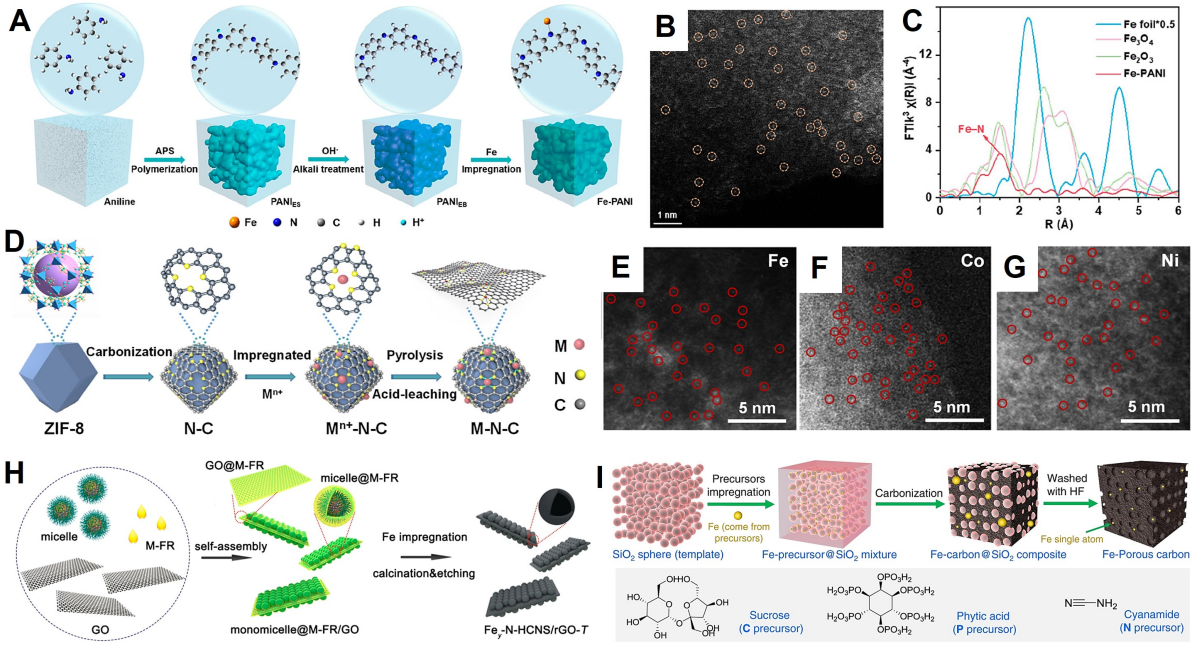

Figure 3. (A) Schematic illustration of the Fe-PANI preparation; (B) AC HAADF-STEM image of Fe-PANI; (C) FT-EXAFS spectra of Fe-PANI. The (A-C) are quoted with permission from Shi *et al.*[55]; (D) Synthesis procedure of M-N-C (M: Fe, Co, Ni) SACs; (E-G) HAADF-STEM images of Fe-N-C, Co-N-C, Ni-N-C. The (D-G) are quoted with permission from Wang *et al.*[52]; (H) Illustration of the synthesis process used to prepare 2D Fe_y-N-HCNS/rGO-T nanosheets. This figure is quoted with permission from Tan *et al.*[56]; (I) Schematic illustration of the preparation process of PCCs. This figure is quoted with permission from Long *et al.*[10]. FT-EXAFS: Fourier transform of extended X-ray absorption fine structure; AC HAADF-STEM: Aberration-corrected high-angle annular dark field scanning transmission electron microscopy; PANI: Polyaniline; SACs: Single-atom catalysts; PCCs: Porous carbon catalysts.

In most cases, the impregnation method needs to be combined with pyrolysis, due to the relatively weak bonding between metal atoms and the support material solely achieved through the impregnation process. Weak interaction can easily cause the dissolution of ions in the catalytic process, so pyrolysis is needed to strengthen this interaction. However, the pyrolysis process is prone to agglomeration of metal substances, necessitating a subsequent acid etching step to dissolve these clusters. MOFs are the precursor materials commonly used in impregnation method. When MOFs are mixed with different metal atomic solutions, various metal SACs with the same structural type can be successfully prepared if these metals have a compatible coordination environment. For example, Wang *et al.*[52] carbonized ZIF-8 to obtain a N-C containing precursor, which was then impregnated into different metal solutions of Fe, Co, and Ni. After pyrolysis and acid etching, M-N-C SACs (M=Fe, Co, Ni) were obtained [Figure 3D-G]. Organic matter is also a support precursor. For example, Tan *et al.*[56] chose triblock copolymer micelles and melamine-formaldehyde resin (M-FR) as precursors to mix with aqueous graphene oxide (GO) solution to get sandwich-like nanosheets (monomicelle@M-FR/GO). After absorbing Fe species through impregnation process, Fe_y-hollow nitrogen-doped carbon nanospheres (N-HCNS)/reduced GO (rGO)-*T* containing only Fe-N(C) bonds but no Fe-Fe bonds were obtained by calcination and acid etching [Figure 3H]. When the precursor contains N element, the M-N-C type catalyst is prepared; when the precursor contains other elements that can bond with metals, the corresponding type of catalyst can be obtained[57]. For example, when Phytic acid is used as the precursor, the M-P-C type catalyst can be obtained [Figure 3I][10].

CVD

The CVD technique is employed for the fabrication of SACs, leveraging the diffusion and adsorption capabilities of metal vapor onto the support surface. In this process, the metal source is thermally activated

to form a vapor, which subsequently engages in a chemical reaction on the support's surface, accelerating the formation of robust metal-support bonds. The formed metal-support bonds ensure that the metal atoms are anchored onto the support surface as single-atom types[58,59]. The CVD strategy exhibits the advantages of a streamlined preparation process ensuring uniform dispersion of metal atoms, but the diffusion rate and adsorption capacity of metal vapor are affected by many factors, which makes the CVD process difficult to control accurately.

In the CVD process, the metal salt and the support precursor are placed at the upstream and the downstream of the tube furnace, respectively. Currently, metal chloride is the most used metal salt for the preparation of Fe, Co or Ni SACs, primarily because metal chloride generally exhibits high volatility, and facile transforms from solid state to gaseous state under heating conditions. In addition, the metal chloride vapor is easy to decompose and release metal atoms at high temperatures. Yuan *et al.*[60] chose $CoCl_2·6H_2O$ as the metal source and carboxylate/amide mixed ligand zinc MOF (DMOF) as the precursor for the support. They successfully prepared Co SACs (Co@DMOF-900) through a gas-phase decarboxylation-induced defect strategy [Figure 4A]. During the CVD process, the decarboxylation increased the defect density of the catalyst, subsequently enhancing the loading rate of Co atoms. The AC HAADF-STEM [Figure 4B] and FT-EXAFS [Figure 4C] images reveal the presence of abundant isolated bright dots in the carbon sheet and the existence of Co-N bonds, suggesting the Co SAs are coordinated with four N atoms to form $Co\text{-}N_4$ bonds. Zhao *et al.*[61] selected $NiCl_2$ as the metal salt to prepare Ni SACs [Figure 4D]. The HAADF-STEM, AC HAADF-STEM, and 3D atom-overlapping Gaussian-function fitting mapping images confirm the successful preparation of Ni SAs [Figure 4E-G]. The FT-EXAFS spectra [Figure 4H] indicate the presence of Ni-N bonds. Apart from chloride salts, Ferrocene can also be used as a metal source in the preparation of Fe SACs. During the pyrolysis process, Fe atoms are coordinated by the N-vacancy derived from Zn evaporation [Figure 4I]. The AC HAADF-STEM image [Figure 4J] and FT-EXAFS spectra [Figure 4K] demonstrate the successful preparation of Fe SACs[22].

ALD

ALD is a cutting-edge technology for preparing thin films that relies on a successive gas-solid phase reaction to achieve film growth layer by layer through chemical deposition. This method is highly suitable for the precise and controlled deposition of either single or multiple layers of metal atoms onto the surface of the support. ALD technology enables the metal atoms to be deposited layer by layer on the surface of the support by alternately introducing metal precursors and reducing agents, thereby obtaining highly dispersed SACs[62,63]. It should be noted that although this technology has the advantages of a precise and controllable deposition process and uniform dispersion of metal atoms, it is associated with high equipment costs and slow deposition rates.

In the process of preparing SACs with ALD, the support can be metal[64], carbon material[65], oxide[66], and so on. The selection of the support material plays a pivotal role in determining the overall performance and stability of the catalyst. In their study, Wang *et al.*[67] successfully deposited Fe SACs onto three distinct support materials: SiO_2, TiO_2, and multi-walled CNTs, and investigated the effect of the support on the catalytic performance. The study displayed that Fe/SiO_2 SACs exhibited excellent CO oxidation reaction performance, mainly owing to the high dispersion and stability of Fe SAs on SiO_2. In the photocatalytic degradation of methylene blue (MB), Fe/TiO_2 SACs demonstrated high photocatalytic activity.

During the ALD process, when metal precursor molecules are deposited on the surface of the support, they often carry undesirable organic ligands. If these ligands remain on the surface of the catalyst, they may impede the exposure of active sites and diminish the catalytic activity. Therefore, it is essential to introduce

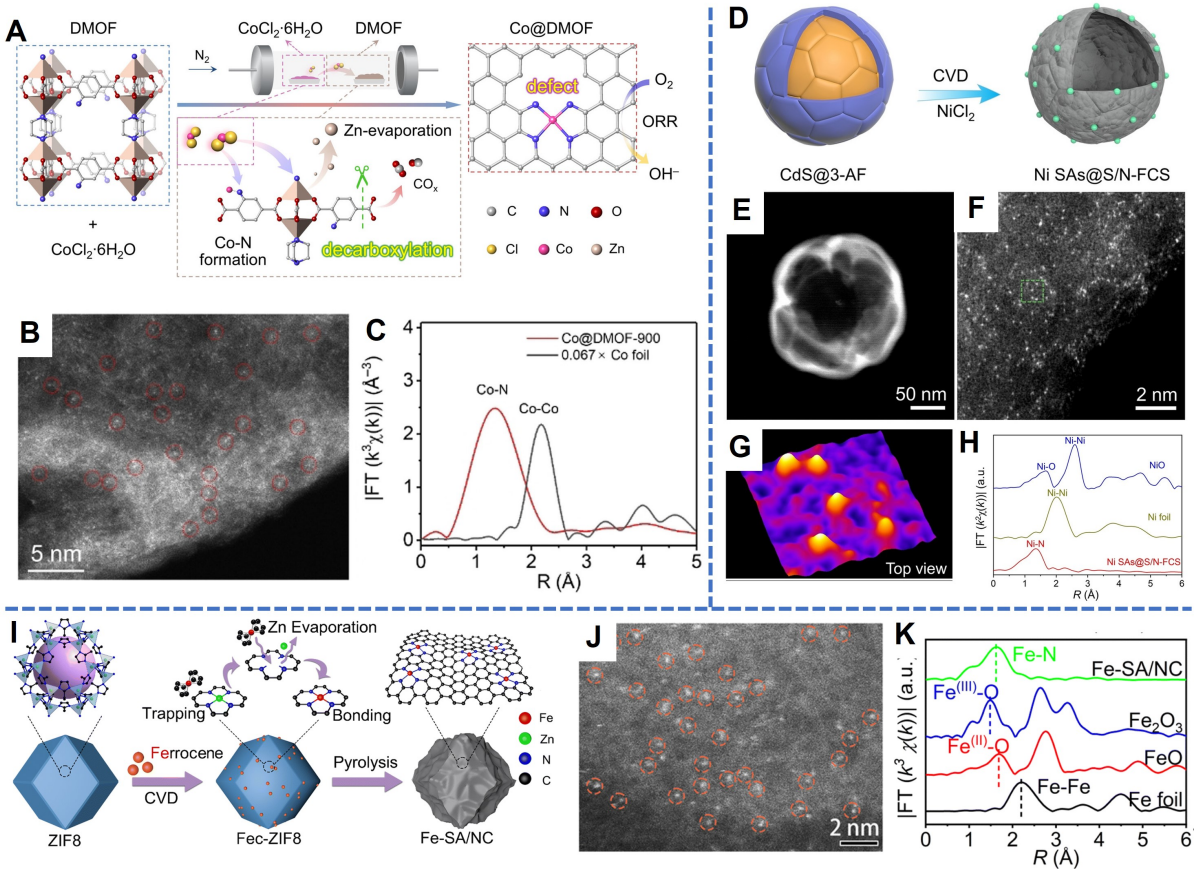

Figure 4. (A) Preparation process and proposed formation mechanisms of Co@DMOF; (B) AC HAADF-STEM; (C) FT-EXAFS curves of Co foil and Co@DMOF-900. The (A-C) are quoted with permission from Yuan *et al.*[60]; (D) Schematic of the synthetic process for the Ni SAs@S/N-FCS; (E) HAADF-STEM and (F) AC HAADF-STEM images of Ni SAs@S/N-FCS; (G) Top view image of 3D atom-overlapping Gaussian-function fitting mapping; (H) FT EXAFS spectra of NiO, Ni foil, and Ni SAs@S/N-FCS. The (D-H) are quoted with permission from Zhao *et al.*[61]; (I) Schematic illustration of the synthesis process for Fe-SA/NC catalysts; (J) AC-HADDF STEM and (K) FT-EXAFS images of Fe-SA/NC catalysts. The (I-K) are quoted with permission from Tian *et al.*[22]. AC HAADF-STEM: Aberration-corrected high-angle annular dark field scanning transmission electron microscopy; FT-EXAFS: Fourier transform of extended X-ray absorption fine structure.

substances that can eliminate these ligands, such as H_2[67], O_2[66], and O_3[68]. In research of Yan *et al.*[68], it was discovered that the introduction of O_3 not only removed the residual ligands from the $Co(C_5H_5)_2$ precursors but also introduced uniform epoxy functional groups on the surface of the GR support. These epoxy functional groups acted as anchor points for Co SAs, enabling their uniform dispersion on GR [Figure 5A] and creating favorable conditions for the subsequent deposition of Co atoms, allowing precise control over the loading amount of Co SAs on GR. Even at a loading of 2.5 wt% [Figure 5B], the cobalt remained in the single-atom state. Electron energy loss spectroscopy (EELS) analysis revealed that oxygen atoms served as effective anchors to secure the Co SAs onto the GR surface [Figure 5C]. Furthermore, FT-EXAFS spectra validated that the cobalt was in an oxidized state rather than a metallic state [Figure 5D]. These two pieces of evidence reinforced the conclusion that the cobalt was indeed in a single-atom state. By regulating the cycle numbers of ALD, it is feasible to exactly control the quantity and density of active sites by atomic-level tuning. Bu *et al.*[69] set the ALD cycle numbers to 1, 5, 10, and 20, and prepared Fe SAs, dimers, trimers, and tetramers, respectively [Figure 5E]. FT-EXAFS analysis [Figure 5F] indicated that when the ALD cycle was completed once, Fe atoms were atomically dispersed. As the number of cycles increased, Fe-Fe bond peaks gradually emerged and their intensities strengthened, suggesting the formation of Fe clusters. Meanwhile,

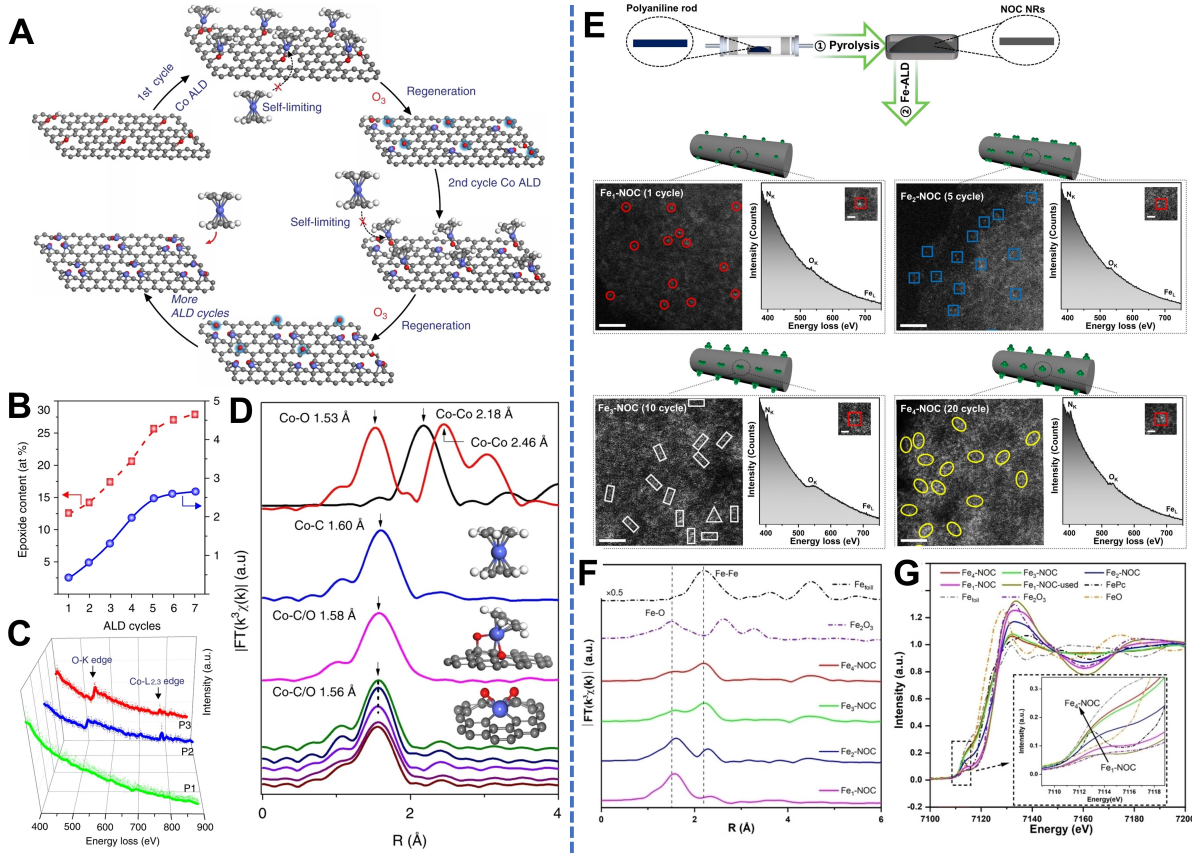

Figure 5. (A) Schematic illustration of the synthesis of Co_1/G SACs with tuneable loadings; (B) Evolution of Co loadings of Co_1/G SACs and epoxy content in graphene as a function of the number of ALD cycles; (C) EEL spectra of O K-edge and Co $L_{2,3}$-edge acquired in the bare graphene region; (D) FT-EXAFS of CoCp/G, Co_1/G SACs with the corresponding structures. The (A-D) are quoted with permission from Yan *et al.*[68]; (E) Illustration of preparation, AC-HAADF-STEM images, and EELS spectra of Fe_x-NOC (x = 1, 2, 3, 4); (F) FT-EXAFS signals of Fe catalysts along with reference samples (dashed lines); (G) XANES spectra at the Fe K-edge of the Fe_x-NOC, Fe foil, Fe_2O_3, FePc, and FeO. The (E-G) are quoted with permission from Bu *et al.*[69]. SACs: Single-atom catalysts; ALD: Atomic layer deposition; EELS: Electron energy loss spectroscopy; FT-EXAFS: Fourier transform of extended X-ray absorption fine structure; AC-HAADF-STEM: Aberration-corrected high-angle annular dark field scanning transmission electron microscopy; XANES: X-ray absorption near edge structure.

XANES spectra [Figure 5G] revealed that as the number of Fe atoms increased, the metallicity of the Fe species enhanced.

Other methods

In addition to the above methods, various strategies exist for the preparation of SACs, such as ball milling, photochemical reduction, electrospinning, templating, and so on. Ball milling is a mechanical method to mix the metal precursor and the support material evenly, which can directly obtain the SACs. Jin *et al.*[70] used this method to prepare Co SACs supported by nitrogen-doped carbon in one step [Figure 6A]. Photochemical reduction is an innovative method that harnesses the power of light energy to facilitate chemical transformations, specifically converting metal ions into single metal atoms and subsequently anchoring them onto a supportive substrate. Zhao *et al.*[71] added frozen $CoCl_2$ aqueous solution in the form of ice cubes to different types of MXene (V_2CT_x, Nb_2CT_x, $Ti_3C_2T_x$) aqueous solutions and maintained them at 0 °C to allow for the slow release of Co^{2+} ions. After removing the residual ice cubes, the mixture was subjected to ultraviolet light irradiation, which reduced and deposited the Co^{2+} ions as single atoms on the MXene substrate [Figure 6B]. Electrospinning is a method that involves incorporating metal salts into a

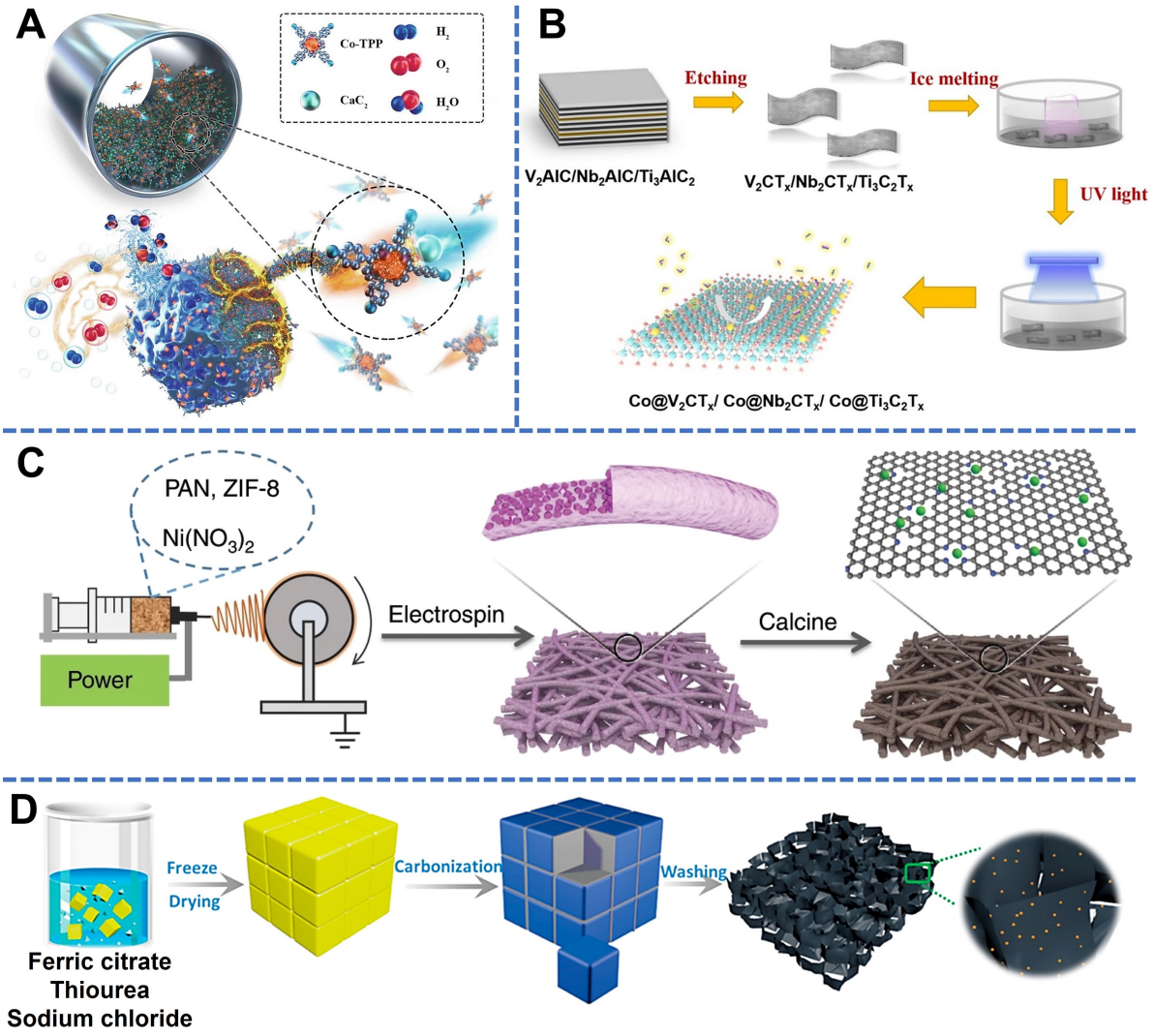

Figure 6. (A) Synthetic protocol for Co-BM-C. This figure is quoted with permission from Jin *et al.*[70]; (B) Schematic illustration of the synthesis procedure of Co@MXenes inspired by the iced photochemical reduction method. This figure is quoted with permission from Zhao *et al.*[71]; (C) Synthesis strategy of NiSA/PCFM. This figure is quoted with permission from Yang *et al.*[72]; (D) Schematic illustration showing the synthesis of Fe SACs. This figure is quoted with permission from Wang *et al.*[39]. SACs: Single-atom catalysts; NiSA/PCFM: Single-atom nickel-decorated porous carbon membrane catalyst.

polymer solution to form a precursor solution, which is then converted into fibers using an electrospinning machine. These fibers undergo subsequent heat treatment and other post-processing steps to yield SACs. Yang *et al.*[72] dissolved polyacrylonitrile (PAN), ZIF-8 nanoparticles, and $Ni(NO_3)_3{\cdot}6H_2O$ in N,N-Dimethylformamide (DMF) to create the precursor solution. The solution was then spun into fibers using an electrospinning machine, followed by heat treatment and acid washing to obtain a single-atom nickel-decorated porous carbon membrane catalyst (NiSA/PCFM) [Figure 6C]. The template method for preparing SACs typically utilizes a specific template to control the morphology, size, and dispersion of the catalyst, ensuring that metal atoms are highly dispersed on the support in the form of single atoms. Sodium chloride (NaCl) is a commonly used template due to its ease of removal through washing after preparation. The preparation process generally involves dissolving sodium chloride, metal sources, carbon sources, and/or nitrogen sources in deionized water, followed by freeze-drying, carbonization, and washing to obtain SACs [Figure 6D][39]. Each of these methods has its unique features, making them suitable for different

preparation requirements and conditions.

APPLICATION OF FE, CO, AND NI SACS IN ELECTROCATALYSIS

The application of Fe, Co, and Ni SACs holds a pivotal position for various kinds of electrochemical energy transformation procedures of electrocatalysis, which have extreme significance toward enhancing the utilization rate of energy and alleviating global warming. Combining the advantages of both homogeneous and heterogeneous catalysts, Fe, Co, and Ni SACs exhibit numerous advantages in electrochemical energy conversion, encompassing: (i) Intrinsic high activity: the single-atom active sites of metal species possess robust inherent activity attributed to their unique molecular configurations; (ii) High density of catalytic sites: stemming from the extensive specific surface area of the support materials, the density of exposed catalytic sites is significantly increased; (iii) High catalytic selectivity: the uniform active centers lead to exceptional catalytic selectivity; (iv) Exceptional stability: the robust bonding between the single metal dopants and adjacent anchoring sites ensures remarkable stability during catalytic processes. This section provides a comprehensive overview of the research advancements in Fe, Co, and Ni SACs for catalytic reactions such as HER, OER, ORR, CO_2RR, and NRR.

HER

In recent years, Fe, Co, and Ni SACs have garnered significant interest because of uniform active sites, high catalytic selectivity, efficient atomic utilization, and low cost. They have demonstrated their efficacy in improving the catalytic performance of the HER. Furthermore, Fe, Co, and Ni SACs can provide a wealth of active sites and efficient pathways for electron transfer, which accelerate the electron transfer process in water splitting reactions, significantly improving catalytic efficiency. Therefore, constructing iron-based SACs is viewed as a vital approach to facilitate efficient HER.

The HER occurs at the cathode of an electrolytic cell under acidic conditions, where protons (H^+) originate from H_3O^+. Electrochemical hydrogen evolution generally undergoes three processes. Firstly, the HER mechanism begins with the formation of adsorbed hydrogen atoms (H_{ads}) in the Volmer reaction:

$$\text{Volmer step: } H_3O^+ + e^- \rightarrow H_{ads} + H_2O \quad \text{(Acidic condition)} \tag{1}$$

$$\text{Volmer step: } H_2O + e^- \rightarrow H_{ads} + OH^- \quad \text{(Alkaline condition)} \tag{2}$$

(Electrochemical hydrogen adsorption)

$$\text{Heyrovsky step: } H_3O^+ + e^- + H_{ads} \rightarrow H_2 + H_2O \quad \text{(Acidic condition)} \tag{3}$$

$$\text{Heyrovsky step: } H_2O + e^- + H_{ads} \rightarrow H_2 + OH^- \quad \text{(Alkaline condition)} \tag{4}$$

(Electrochemical desorption)

$$\text{Tafel step: } H_{ads} + H_{ads} \rightarrow H_2 \tag{5}$$

(Complex desorption)

In the whole process of hydrogen evolution, a predominance of the adsorption phase over the desorption phase facilitates hydrogen formation but obstructs its release. On the contrary, a weak adsorption promotes

hydrogen generation. Optimal hydrogen evolution activity is achieved only when a proper equilibrium between these two processes exists. The Gibbs free energy (ΔG) associated with hydrogen adsorption is typically utilized as an indicator of the catalyst's efficacy; values close to zero indicate a more favorable HER.

However, when hydrolytic dissociation requires a high energy barrier and hydrogen desorption is challenging, HER activity is hindered. In this regard, electronic regulation of the catalyst is proposed as a strategy for enhancing HER performance. For example, doping Ni into MoB_2 has been shown to optimize the HER. The remarkable electrocatalytic activity for hydrogen evolution is attributed to the adjustment of the electronic structure of the Mo site on the Ni-MoB_2 surface, facilitated by the presence of Ni atoms, which promotes the dissociation of H_2O[13].

In recent years, the introduction of a high density of single atomic sites in the carrier to obtain the highest atomic efficiency and enhanced catalytic performance has become a forefront approach[33]. Among them, the carrier can be carbon materials, but non-carbon materials are currently popular and show higher catalytic effects, such as hydroxides, oxides, nitrides, sulfides and phosphates[15]. Gong *et al.*[73] proposed a comprehensive sub-nanoreactor approach to synthesize a single atomic electrocatalyst supported by MoS_2 in egg yolk shells, thereby achieving a powerful HER. As illustrated in Figure 7A, it can be clearly observed that most of the Co atoms can be integrated into the expansion layer of the C-MoS_2 carrier. The Co Kedge X-ray absorption fine structure (XAFS) was tested to elucidate Co's valence and structure. The findings indicate that the absorption edge of C-Co-MoS_2 is positioned between that of Co foil and the CoO, confirming that the Co valence state is + 1.75 [Figure 7B]. As shown in Figure 7C, the sample of C-Co-MoS_2 exhibited no Co-Co peak, suggesting that Co predominantly exists as isolated atoms. The C-Co-MoS_2 catalyst demonstrates an overpotential of 17 mV and an ultra-low Tafel slope at 10 mA/cm^2, which is much better than other double-anchored MoS_2 electrocatalysts [Figure 7D and E]. Notably, C-Co-MoS_2 showed superior activity than commercial Pt/C, indicating enhanced HER performance over other C-M-MoS_2 (M=Mn, Ni, and Fe). The computed results agree with the experimental results [Figure 7F]. Fe SACs not only show outstanding performance in sulfides but also improve catalytic performance in oxide matrices. In order to explore the actual catalytic activity center of C-Co-MoS_2, density functional theory (DFT) calculation was performed for the material. Four possible hydrogen absorption sites of S, C, Co and Mo were calculated, and the $\Delta G_H^{(1)}$ and $\Delta G_H^{(2)}$ of Co sites were calculated to be 0.19 and -0.12 eV, respectively, which were lower than other sites. The highest log (i_0) value indicates that the thermodynamic process of hydrogen adsorption-desorption at the Co site is relatively simple, and the real catalytic center may be the Co site. The electron change between Co and H was subsequently investigated in the C-Co-Mo model. After the first H atom adsorption, the electron density around Co atoms increased, which was conductive to adsorb the second H atom. Then, the electron density of Co decreased when adsorbing the second H atom, which could be attributed to the electron transfer from Co to H in the cathodic reaction. Shah *et al.*[29] prepared Co SACs supported on spherical RuO_2, demonstrating them as efficient and stable HER catalysts, in which the Co SACs supported on spherical RuO_2 could be confirmed by aberration corrected scanning transmission electron microscopy (AC-STEM), X-ray photoelectron spectroscopy (XPS) and X-ray absorption spectroscopy (XAS) [Figure 7G-K]. At a current density of 10 mA/cm^2, the catalyst only needs a 45 mV overpotential to drive the HER process and has an ultra-low Tafel slope [Figure 7L and M]. Theoretical calculation shows that the energy barrier of HER will be reduced after the addition of Co SACs, which significantly improves the activity of Ru-based electrocatalysts in acidic conditions [Figure 7N].

In conclusion, the high activity, stability, low cost, and controllability of iron monatomic catalysts in HER catalysis make it a promising alternative catalyst. They are anticipated to play an important role in electrolysis for hydropower electrolysis and other related energy conversion[74,75].

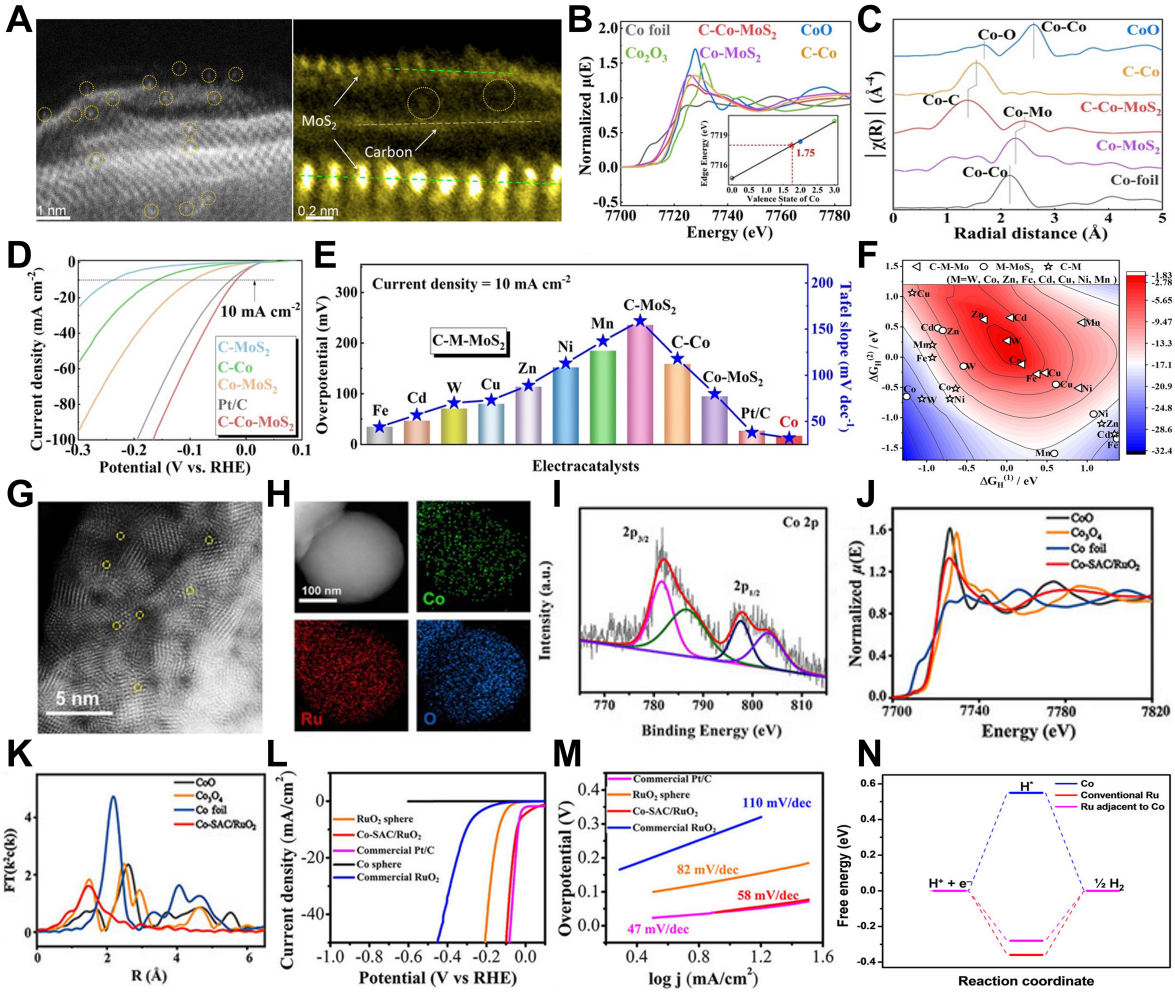

Figure 7. (A) HRTEM and AC-TEM images of the C-Co-MoS_2; (B) Fitting curve of EXAFS spectra for Co in R space; (C) Wavelet Transform (WT) of the Co K-edge; (D) Polarization curves of the C-MoS_2, single-anchored, and dual-anchored electrodes; (E) Overview of overpotentials and Tafel slopes; (F) 3D volcano plot with $\Delta G_H^{(1)}$, $\Delta G_H^{(2)}$), and log (i_0) for the C-M-Mo, M-MoS_2, and C-M. The (A-F) are quoted with permission from Gong *et al.*[73]; (G) AC HAADF-STEM image; (H) STEM image and EDX elemental mapping of Co-SAC/RuO_2; (I) XPS profiles of Co 2p; (J) XANES spectra at the Co K-edge; (K) WT analysis of Co K-edge; (L) LSV curves; (M) Tafel slopes; (N) Free energy profile of HER. The (G-N) are quoted with permission from Shah *et al.*[29]. HRTEM: High resolution transmission electron microscope; TEM: Transmission electron microscopy; STEM: Scanning transmission electron microscopy; EDX: Energy-dispersive X-ray; XPS: X-ray photoelectron spectroscopy; AC-HAADF-STEM: Aberration-corrected high-angle annular dark field scanning transmission electron microscopy; XANES: X-ray absorption near edge structure; WT: Wavelet-transformed; LSV: Linear sweep voltammetry; HER: Hydrogen evolution reaction; EXAFS: Extended X-ray absorption fine structure.

OER

The reaction for the OER has consistently been a crucial factor limiting the overall efficiency of water electrolysis systems. This process involves hydroxide ions or water losing electrons to produce oxygen, typically taking place at the anode of the electrolytic cell. The specific reaction process is as follows:

Alkaline condition:

$$OH^- + * \rightarrow OH_{ads} + e^- \quad (6)$$

$$OH_{ads} + OH^- \rightarrow O_{ads} + H_2O + e^- \quad (7)$$

$$O_{ads} + OH^- \rightarrow OOH_{ads} + e^- \quad (8)$$

$$OOH_{ads} + OH^- \rightarrow O_{2ads} + H_2O + e^- \quad (9)$$

$$O_{2ads} \rightarrow O_2 + * \quad (10)$$

Acidic condition:

$$H_2O + * \rightarrow OH_{ads} + H^+ + e^- \quad (11)$$

$$OH_{ads} \rightarrow O_{ads} + H^+ + e^- \quad (12)$$

$$O_{ads} + H_2O \rightarrow OOH_{ads} + H^+ + e^- \quad (13)$$

$$OOH_{ads} \rightarrow O_{2ads} + H^+ + e^- \quad (14)$$

$$O_{2ads} \rightarrow O_2 + * \quad (15)$$

Studies have shown that the OER usually occurs on the oxide layer or hydroxyl oxide formed on the catalyst surface, and its activity is mainly based on the adsorption evolution mechanism (AEM) and lattice oxygen mechanism (LOM). Unlike previous adsorption mechanisms, the LOM usually involves a catalyst being adsorbed on the surface and acquiring an electron from the electrode surface, resulting in the surface lattice oxygen becoming a positively charged active species.

However, the energy barrier caused by the multi-step proton-coupled electron transfer mechanism significantly hinders the kinetic process, resulting in the demanded current density to be reached at a higher overpotential. So far, Ru/IR-based oxides have been proven to be the benchmark of OER electrocatalysts[66], but they have problems of high cost and poor stability, so it is particularly important to find a catalyst with excellent activity. The significant advantages of SACs lie in their exceptional atom utilization efficiency, high uniformity of metal active centers, and the tunability of their coordination environments, making them highly desirable for various applications[76].

For example, Wang *et al.*[66] developed a stable and atomically dispersed iron SAC confined in a covalent organic framework (Fe-SAC@COF) catalyst that uses XAFS spectroscopy to investigate the interface structure at the atomic level. The XANES spectrum of the Fe-SAC@COF sample is located between the corresponding metal foil and the metal oxide [Figure 8A], indicating that the metal atoms in the COF are in an oxidized state. In addition, the metal coordination environment was confirmed using FT-EXAFS spectroscopy. As shown in Figure 8B, only a main peak attributed to the Fe-N/O scattering path (1.47 Å) is presented and no Fe-Fe bond (2.17 Å) is detected. This result conclusively verifies that the Fe atoms in Fe-SAC@COF exist in the form of single atoms. The experimental test results also show that the overpotential of Fe-SAC@COF electrodes is only 290 mV when the current density reaches 10 mA cm^{-1}, which proves the excellent performance of the Fe monatomic catalyst [Figure 8C].

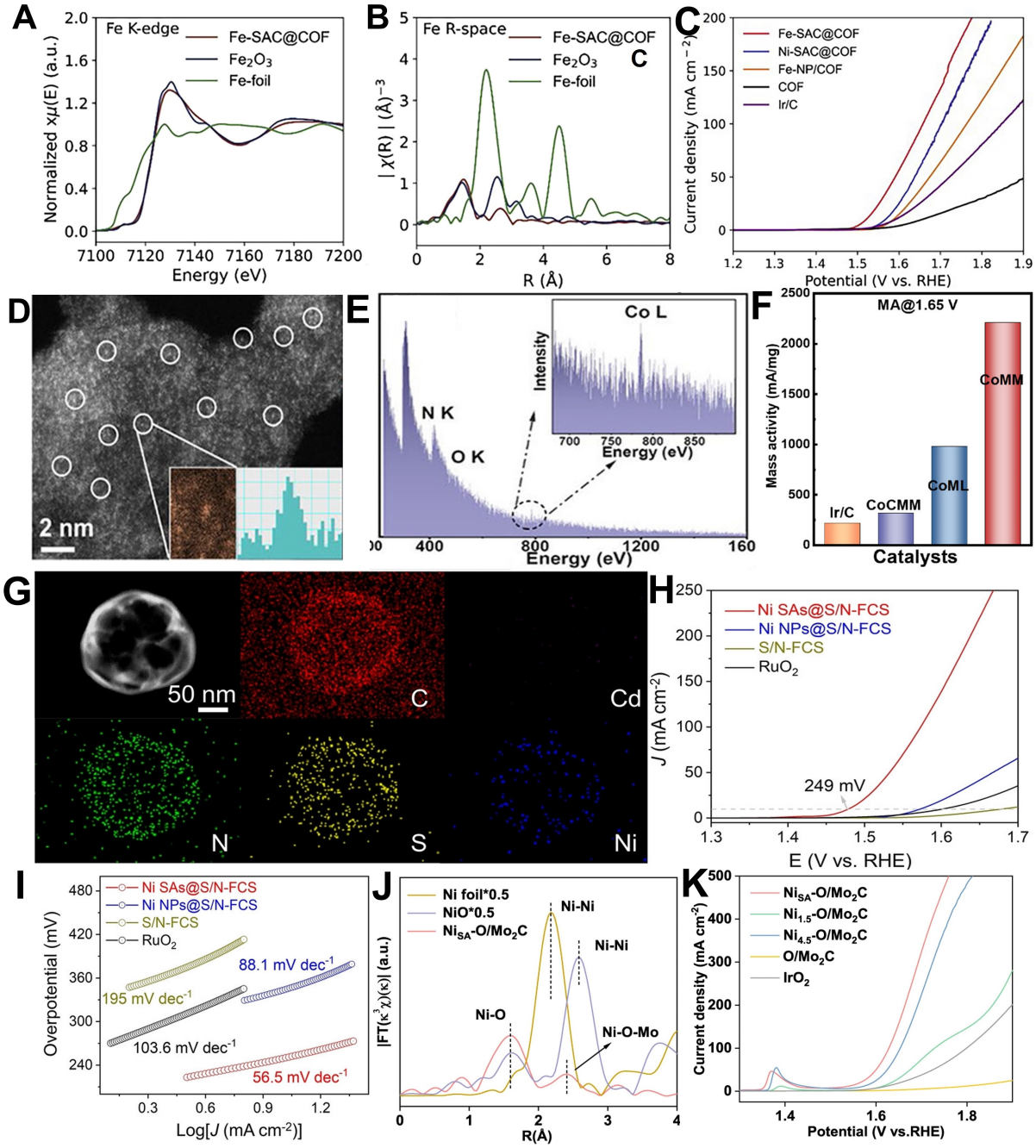

Figure 8. (A) K-edge XANES spectra of Fe-SAC@COF; (B) Fourier transform EXAFS spectra of Fe-SAC@COF and reference sample; (C) LSV curves of Fe-SAC@COF and reference samples in OER. The (A-C) are quoted with permission from Wang *et al.*[66]; (D) AC HAADF STEM image of CoMM; (E) EELS spectrum of CoMM; (F) Mass activity of OER electrocatalyzed by cobalt-based electrodes. The (D-F) are quoted with permission from Kumar *et al.*[77]; (G) Mapping images of corresponding elements of HAADF-STEM and individual Ni SAs@S/N-FCS; (H) OER polarization curve of Ni SA@S/N-FCS; (I) Corresponding Tafel slopes of RuO_2, S/N-FCS, Ni NPs@S/N-FCS and Ni SA@S /N-FCS. The (G-I) are quoted with permission from Zhao *et al.*[61]; (J) FT-EXAFS curve of Ni_{SA}-O/Mo_2C; (K) OER polarization curve of Ni_{SA}-O/Mo_2C. The (J-K) are quoted with permission from Hou *et al.*[78]. XANES: X-ray absorption near edge structure; EXAFS: Extended X-ray absorption fine structure; OER: Oxygen evolution reaction; AC HAADF STEM: Aberration-corrected high-angle annular dark field scanning transmission electron microscopy; CoMM: Graphenic network using melem; EELS: Electron energy loss spectroscopy; LSV: Linear sweep voltammetry; SACs: Single-atom catalysts; COF: Covalent organic framework.

Moreover, Co SACs are also a promising catalyst in OER process. This work utilized an AC-HAADF-STEM

to investigate the ultrafine morphological characteristics of Co-N4 (pyridinic) porous graphenic network using melem (CoMM) and Co-N4 (pyridinic) graphene network using melamine (CoML), which demonstrated the presence of Co SAs with distinct Z-contrast on C-N scaffolds, with no observable clusters [Figure 8D]. The small-pixel EELS spectrum of the annular dark field (ADF) image clearly detected Co and N signals, confirming the presence of dense Co in the C-N network [Figure 8E]. Figure 8F revealed that Co-N_4 SAC catalyst can achieve a mass activity/turnover frequency (TOF) of up to 2,209 mA mg_{Co}^{-1} at 1.65 V/ 0.37 s^{-1}. This is due to the low free energy variation and good electron transport of the CO-N_4 SAC catalyst, while the separated Co center also effectively promotes an efficient and stable (> 300 h) electrocatalytic OER process[77].

In 2022, the hollow S/N-doped football-shaped carbon spheres modified by single Ni atoms (Ni SAs@S/N-FCS) were designed and prepared by Zhao *et al.*[61]. A large number of exposed single Ni sites on the surface and hollow S/N-doped carbon structures greatly improve the catalytic activity of the catalyst in the OER. The large distribution of Ni elements in the element map in Figure 8G also proves that a lot of Ni sites exist in this catalyst to a certain extent. Meanwhile, Figure 8H also shows that when the current density reaches 10 mA cm^{-2}, the overpotential is only 249 mV, and the Tafel slope is 56.5 $mVdec^{-1}$ [Figure 8I], indicating that the reaction kinetics of the catalyst is fast.

In addition, Hou *et al.*[78] just reported the excellent performance of Ni monatomic catalysts in HER and OER in 2024, providing guidance for the design and preparation of monatomic bifunctional catalysts. The research team engineered a non-precious metal Ni single-atom bifunctional catalyst (Ni_{SA}-O/Mo_2C) that is anchored on an oxygenated Mo_2C surface through Ni-O-Mo bridge bonds. As shown in Figure 8J, a prominent peak attributed to the Ni-O bond was detected around 1.58 Å, while the peaks located at 2.18 Å and 2.58 Å detected in the Ni foil and NiO samples, respectively, were assigned to Ni-Ni interactions. The absence of such peaks in the Ni_{SA}-O/Mo_2C sample indicates that the Ni atoms are present as isolated form atop the amorphous MoO_x thin layer. Figure 8K shows that the OER overpotential of the Ni_{SA}-O/Mo_2C catalyst is 299 mV at a current density of 10 mA cm^{-2} during the reaction of the electrode material. Meanwhile, the Potential Determining Step (PDS) for OER is the third electrochemical step from *O to *OOH. Through calculation, Ni_{SA}-O/Mo_2C remarkably decreases the energy barrier in this step to 1.61 eV, lower than that of O/Mo_2C (1.84 eV) and Ni_{SA}-Mo_2C (2.69 eV) at U = 1.23 V, indicating Ni_{SA}-O/Mo_2C has much better performances, being consistent with the experimental observations. Based on the above results, it would be found that the partially oxidized surface of Mo_2C facilitated the binding of Ni atoms via Ni-O and Ni-Mo (Ni-O-Mo) chemical bonds, thus promoting the electrocatalytic properties of OER.

Modification of precious metal monatoms, clusters and nanoparticles to improve the OER performance of rare earth-rich electrocatalysts has proved to be a promising approach. Specifically, SACs have received widespread attention due to their almost 100% atomic utilization and unprecedented catalytic activity. Therefore, the development of single-metal atomic catalysts still needs to be further explored[73].

ORR

The ORR is a multi-electron reaction involving a series of elementary reactions and intermediate reactions with a relatively complicated mechanism. The mechanism proposed by Wroblowa in 1976 is widely regarded as the most effective explanation of this complex process. In ORR, O_2 diffuses from the solution and adsorbs on the catalyst surface, converting into active oxygen molecules. Two main electron transfer pathways: a four-electron reaction pathway leading to the generation of H_2O in acidic medium or OH^- in alkaline medium as intermediates and a two-electron pathway leading to the generation of H_2O_2 in acidic media or HO- 2 in alkaline medium [Figure 9A][12]. In general, the reduction potential of the four-electron

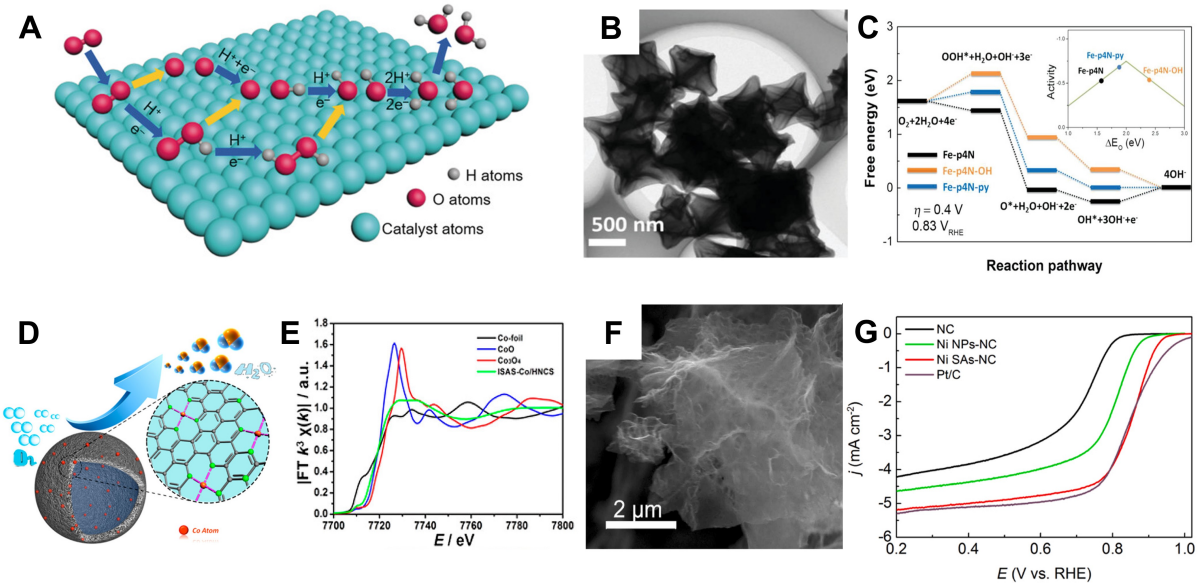

Figure 9. (A) The ORR mechanism is shown with the blue arrow for proton/electron transfer and the yellow arrow for the O-O bond break. The illustration is quoted with permission from Wang *et al.*[12]; (B) Fe SAC/N-C TEM image; (C) Free energy diagrams of the ORR process of three Fe-SACs in different coordination environments at 0.4 V overpotential, and the volcano plot in the upper right corner. The B and C figures are quoted with permission from Lin *et al.*[80]; (D) Illustration of ISAS-Co/HNCS; (E) ISAS-Co/HNCS XANES spectra at the Co K-edge. The D and E are quoted with permission from Han *et al.*[81]; (F) SEM images of Ni SAs-NC; (G) LSV curves of different catalysts in O_2 saturated 0.1 M KOH. The F and G are quoted with permission from Jiang *et al.*[82]. ORR: Oxygen reduction reaction; TEM: Transmission electron microscopy; SACs: Single-atom catalysts; ISAS-Co/HNCS: Isolated single atomic sites are dispersed on hollow N-doped carbon spheres; XANES: X-ray absorption near edge structure; SEM: Scanning electron microscopy; Ni SAs-NC: Ni SAs dispersed on N-doped carbon nanosheets; SV:

reaction is higher than the two-electron reaction. The specific reaction mechanism for this reaction is as follows:

Four-electron reaction:

Acidic condition:

$$O_2\,(g) + 4H^+\,(aq) + 4e^- \rightarrow 2H_2O\,(l) \tag{16}$$

Alkaline condition:

$$O_2\,(g) + 2H_2O\,(l) + 4e^- \rightarrow 4OH^-\,(aq) \tag{17}$$

Two-electron reaction:

Acidic condition:

$$O_2\,(g) + 2H^+\,(aq) + 2e^- \rightarrow H_2O_2\,(l) \tag{18}$$

$$H_2O_2\,(l) + 2H^+\,(aq) + 2e^- \rightarrow 2H_2O\,(l) \tag{19}$$

Alkaline condition:

$$O_2\ (g) + H_2O\ (l) + 2e^- \rightarrow HO_2^-\ (aq) + OH^-\ (aq) \quad (20)$$

$$HO_2^-\ (aq) + H_2O\ (l) + 2e^- \rightarrow 3OH^-\ (aq) \quad (21)$$

In materials with weaker catalytic activity, there may be a tendency towards two-electron reactions or a mixture of two- and four-electron reactions, which could lead to the formation of peroxides, potentially damaging the catalyst and the proton exchange membrane. However, the four-electron reaction pathway completely reduces O_2 to H_2O, avoiding the formation of hydrogen peroxide and increasing current efficiency. Therefore, the four-electron reaction is recognized as the most optimal pathway for the ORR process.

In 1964, Jasinski *et al.*[79] investigated the electrocatalytic effect of cobalt phthalocyanine (CoPc) on ORR, which marked the M-N-C catalysis discovery. These catalysts have demonstrated high catalytic activity for multiple steps of the ORR and are widely recognized as ideal oxygen reduction catalysts. In particular, Fe and N-doped carbon catalysts have become the focus of current research on transition metal catalysts due to their exceptional ORR activity and four-electron selectivity. Recently, some representative design strategies have enhanced the activity of transition metal SACs in ORR. Lin *et al.*[80] have used an open framework with chelating ligands that can insert metal ions exactly at the desired positions and effectively avoid the formation of useless products to successfully construct several stable metal SACs (SACs/N-C) (metal=Fe, Co, Ni, *etc.*). Experiments indicate that the pure N-C site itself has very weak ORR activity, confirming the high ORR activity is due to the metal single-atom sites. These Fe SAC/N-C catalysts have a highly open porous structure [Figure 9B], facilitating full exposure and transport of active sites, and exhibit excellent oxygen reduction activity ($E_{1/2}$ of 0.89 V, 40 mV higher than commercial Pt/C) [Figure 9C] and excellent stability. However, despite the clear performance advantages of Fe SAC/N-C electrocatalysts, their limited stability continues to pose a significant challenge to practical applications. These catalysts are susceptible to the Fenton reaction, where intermediates generated at the Fe sites contain a high concentration of reactive oxygen species that rapidly reduce the carbon matrix activity, accelerating the decay of catalyst activity.

Co is also a widely utilized transition metal, highly favored for its exceptional catalytic activity and chemical stability. Unlike Fe SACs that easily initiate the Fenton reaction, Co SACs do not cause such side reactions. Han *et al.*[81] have successfully fabricated a Co catalyst in which isolated single atomic sites are dispersed on hollow N-doped carbon spheres (ISAS-Co/HNCS) through a pyrolysis method. This structure not only achieves dispersed Co atom sites but also increases active site exposure, which promotes the transport of species related to ORR [Figure 9D]. The result shows that ISAS-Co/HNCS had excellent ORR activity ($E_{1/2}$ = 0.773 V), close to the level of Pt/C catalysts and significantly exceeding the cobalt-free hollow N-doped carbon spheres [Figure 9E]. Furthermore, ISAS-Co/HNCS exhibits excellent anti-methanol toxicity in combination with excellent stability. Under 1.0 M MeOH, the current change is almost insignificant, and the ORR polarization curve is almost not shifted after 10,000 cycles. The enhanced ORR activity can be largely credited to the well-distributed cobalt atomic positions, which facilitate a marked increase in the rate of OH* hydrogenation. To explore the origin of the high ORR reactivity of ISAS-Co/HNCS, DFT calculations were carried out. On ISAS-Co/HNCS catalyst, all the electron-transfer steps are exothermic at U = 0 V, and thus the free energy pathway is downhill. With the potential increased to above 0.54 V, the first reduction step (i.e., O_2* + H+ + e^-→ OOH*) and the last electron-transfer step (i.e., OH* + H^+ + e^- → H_2 O) become endothermic in succession. In contrast, it is shown that even at U = 0 V on Co particles, the first and last reduction steps are endothermic by 0.17 and 0.63 eV, respectively. This suggests that Co particles

should exhibit much less reactivity than ISAS-Co/HNCS. According to the free energetics, the rate-determining step (RDS) on Co particles is the last reduction step. Therefore, the high ORR reactivity of ISAS-Co/HNCS is attributed to the significant improvement of the last elementary step at the single Co site, which facilitates the proton and charge transfer to the adsorbed *OH species. Experiments and DFT have verified that isolated Co sites are the source for the high ORR activity because they significantly increase the hydrogenation of OH* species. This template-assisted pyrolysis (TAP) method is also demonstrated to be effective in preparing a series of ISAS-M/HNCS, which provides opportunities for discovering new catalysts.

Nickel metal is also usually used for four-electron ORR reactions, but further development of this site has been impeded by the relatively weak oxygen binding capacity of NiN_4. The results show that precisely modulating the Ni-N-C coordination environment can effectively narrow at the Ni-based centers and oxygen intermediates the energy barrier, thereby enhancing their oxygen reduction capabilities. By individually anchoring Ni SAs dispersed on N-doped carbon nanosheets (Ni SAs-NC), Jiang *et al.*[82] have developed a new bifunctional electrocatalyst that supports both ORR and urea oxidation reactions [Figure 9F]. Owing to the high dispersion and full exposure of the Ni-N_4 sites, Ni SAs-NC exhibits larger specific surface area and pore volume compared to Ni NPs-NC and NC, facilitating the transfer of ions and protons during the electrocatalysis process. The Ni SAs-NC catalyst demonstrates excellent bifunctional catalytic activity and stability ($E_{1/2}$ of 0.85 V), comparable to Pt/C, along with much more positive than the values for Ni NPs-NC (0.80 V) and NC (0.71 V) [Figure 9G]. Building upon these findings, the researchers have further successfully developed a rechargeable zinc-air battery (ZAB). After continuous operation for 20 hours, the current retention rate of the ZAB reached 93.7%, which is a 17.1% improvement over traditional ZAB and displays a higher energy conversion efficiency[83-85]. This advancement propels the ZAB technology towards practical applications and offers new opportunities for the design of innovative, high-efficiency electrochemical energy storage materials[79,86,87].

CO_2RR

CO_2, a primary contributor to the greenhouse effect, is experiencing a rise in atmospheric concentration due to the extensive burning of fossil fuels. Owing to its comparatively stable molecular configuration, it is unable to be decreased at normal room temperature[88]. The electrocatalytic CO_2RR technology constitutes an ideal means to reach the objective of "carbon neutrality". Effective CO_2RR electrocatalysts can reduce the energy barrier for CO_2 activation, control the complex synthetic routes, and restrain the competitive side reaction of HER. The SACs of Fe, Co, and Ni, characterized by adjustable electronic configurations, high atomic utilization rates, and uniform active positions, possess considerable advantages in the study of CO_2 RR[19,34,89]. Table 1 presents the half-reactions derived from CO_2RR along with the respective standard potentials [V *vs.* Reversible Hydrogen Electrode (RHE)][90].

Among these, CO, an important chemical intermediate, plays a key role in catalyzing the conversion of CO_2 into usable fuels. Among many possible reaction pathways, the electrochemical CO_2 reduction (ECR) reaction to generate CO only involves two-electron and two-proton transfer, making it less hindered and being considered one of the most industrially promising reactions. This section mainly discusses the reaction site regulation strategy of iron-based single-atom electrocatalysts and the regulation mechanism of electrocatalytic selectivity, with a focus on summarizing the regulation of the intermediate process of proton-coupled CO_2 reduction to generate CO. Electrocatalytic reduction of CO_2 to CO is a process involving the transfer of $2e^-$ and $2H^+$. In the process, CO_2 is first adsorbed on catalyst surfaces and transformed into COOH* intermediates, followed by continued reduction to CO.

Table 1. Electrocatalytic reduction of CO_2 to various products at specific potentials

Reduction	E^0 (V *vs.* RHE)
$CO_2 + e^- \rightarrow CO_2^-$	-0.19
$CO_2 + 2e^- + 2H^+ \rightarrow HCOOH$	-0.12
$CO_2 + 2e^- + 2H^+ \rightarrow H_2O + CO$	-0.10
$CO_2 + 6e^- + 6H^+ \rightarrow 2H_2O + CH_3OH$	+0.03
$CO_2 + 8e^- + 8H^+ \rightarrow 2H_2O + CH_4$	+0.17
$CO_2 + 12e^- + 12H^+ \rightarrow 2H_2O + C_2H_5OH$	+0.09
$CO_2 + 12e^- + 12H^+ \rightarrow 2H_2O + C_2H_4$	+0.08
$CO_2 + 18e^- + 18H^+ \rightarrow 5H_2O + C_3H_7OH$	+0.10

RHE: Reversible hydrogen electrode.

$$1e^- + 1H^+ + CO_2 \rightarrow {}^*COOH \quad (22)$$

$$1e^- + 1H^+ + {}^*COOH \rightarrow H_2O + {}^*CO \quad (23)$$

$${}^*CO \rightarrow {}^* + CO \quad (24)$$

Where "*" indicates the active site on the catalyst surface.

Based on specific reaction pathways, desirable SACs should have appropriate adsorption energies towards key reaction intermediates. For example, using a template approach, Li *et al.*[43] successfully synthesized uniformly dispersed single nickel sites on hollow, porous, urchin-like nitrogen-doped carbon nanostructures [Ni-NC(HPU)]. Electron microscopy characterizations of Ni-NC(HPU) are shown in Figure 10A-D. There were no visible nickel-based aggregates observed in the Dark-field TEM images [Figure 10A and B], indicating the good dispersion of nickel species on the NC matrix. This conclusion was further evidenced by the energy-dispersive X-ray (EDX) spectroscopy elemental mapping images. The nickel, nitrogen and carbon elements were uniformly distributed throughout the entire Ni-NC(HPU) matrix [Figure 10C]. HAADF-STEM observed Ni SAs at the atomic scale [Figure 10D]. [Ni-NC(HPU)] possesses a high degree of crystallinity, which can fully expose the monodispersed Ni sites and concurrently accomplish efficient electron transfer/mass transfer. It performs excellently in CO_2 reduction reactions where it shows great selectivity and a significant increase of CO current density, along with remarkable durability. Pei *et al.*[91] utilized a thermal displacement strategy to synthesize systematically adjusted Co SACs, namely Co-N_4, Co-S_1N_3, Co-S_2N_2, and Co-S_3N_1, and investigated the relationship between their coordination environment and CO_2RR performance. As the Co-S coordination number increases, the binding strength with the CO_2RR intermediate products (*COOH and *CO) constantly weakens. The Co-S_1N_3 SAC lies at the top of the volcano, and the binding force with *COOH and *CO is optimized, possessing high activity and selectivity for the conversion of CO_2RR to CO. Wang *et al.*[52] designed the SACs which automatically adjust the coordination numbers or bond length for the CO_2RR process. The monatomic dispersion of Fe in Fe-N_4, Fe-S_1N_3, and Fe-B_1N_3 was confirmed by Wavelet-transformed (WT)-EXAFS analyses of the Fe K-edge [Figure 10E]. By constructing asymmetrically coordinated Fe SACs possessing dynamically evolving structures, the catalytic activity was successfully enhanced. The prepared catalyst contains an Fe atom coordinated by a S and three N atoms (Fe-S_1N_3) and demonstrates excellent CO selectivity with a Faradaic efficiency (FE) of up to 99.02%, superior activity manifested by a TOF of 7804.34 h^{-1} and outstanding stability. DFT calculations were performed to investigate internal factors responsible for breaking the linear scaling relationship in the electrochemical CO_2RR process, leading to

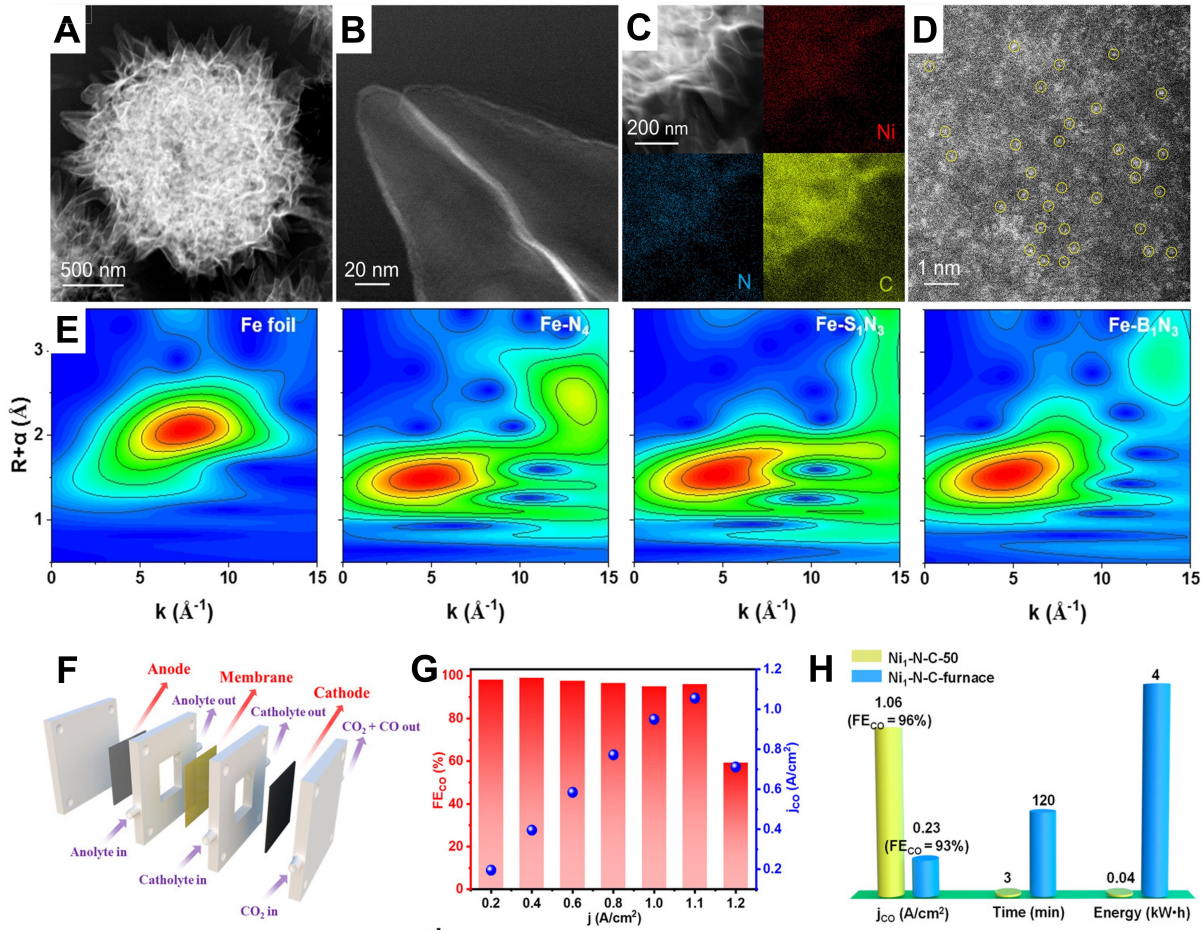

Figure 10. Performance characterization and tests of iron-based (Fe, Co, Ni) single-atom catalysts for carbon dioxide reduction electrocatalysts. (A-D) Dark-field TEM, EDX elemental mapping, and AC HAADF-STEM images of Ni-NC(HPU), respectively. The (A-D) are quoted with permission from Li *et al.*[43]; (E) WT EXAFS of the k^3-weighted k-space spectra of different samples. Fe-N_4, Fe-S_1N_3 and Fe-B_1N_3. This figure is quoted with permission from Wang *et al.*[52]; (F) Schematic illustration of a flow cell with the gas diffusion electrode for CO_2 electroreduction; (G) The values of FE_{CO} and j_{CO} of Ni_1-N-C-50 tested by chronopotentiometric measurements under various current densities; (H) Comparison of j_{CO} (tested in the flow cell), time and energy consumption in the pyrolysis process between Ni_1-N-C-50 and Ni_1-N-C-furnace. The (F-H) are quoted with permission from Wen *et al.*[93]. AC HAADF-STEM: Aberration-corrected high-angle annular dark field scanning transmission electron microscopy; TEM: Transmission electron microscopy; EDX: Energy-dispersive X-ray; WT: Wavelet-transformed; EXAFS: Extended X-ray absorption fine structure.

improved intrinsic activity. The models, including FeN_4, Fe-S_1N_3, and Fe-B_1N_3, were crafted and their veracity established through EXAFS fitting, demonstrating excellent alignment with experimental architectures. The distinctive asymmetric coordination landscape and pronounced geometric distortions at Fe-S_1N_3 sites introduced an asymmetric profile to the lowest unoccupied molecular orbital (LUMO), fostering a superior match with the highest occupied molecular orbital (HOMO) of CO_2. This optimized orbital overlap facilitated the adsorption and activation of CO_2 at Fe-S_1N_3 sites, representing a key step toward enhanced catalysis. Moreover, the analysis unveiled that Fe-S_1N_3 exhibited not only the strongest CO_2 adsorption energy but also the lowest energy barrier for *COOH formation, underlining its unparalleled potential in CO_2 sequestration and activation. The Fe-S_1N_3 site stood out in its capacity to donate electrons most effectively to the *COOH intermediate, while minimizing electron transfer with *CO intermediates. This translated into the highest *COOH adsorption energy among all active sites, further boosting CO_2 activation and *COOH formation. Concurrently, the Fe-S_1N_3 site featured the lowest *CO adsorption energy, thereby expediting *CO desorption, a critical aspect for maintaining catalyst efficiency.

Chen *et al.*[92] disclosed that a notable proton-feeding effect in CO_2RR was produced by sulfur doping. Spectroscopy and microscopy were used to validate the SAC catalyst model of sulfur doping within the FeN_4 (Fe_1-NSC) secondary shell layer. Fe_1-NSC offered much better CO_2RR performance than sulfur-free FeN_4 and Fe-based SACs described in most studies up to the 98.6% CO Faraday efficiency with a ToF of 1197 h^{-1}. Jia *et al.*[36] disclosed a highly ordered hierarchical porous single-atom Fe catalyst for efficient CO_2 electroreduction. The single-atom Fe-N-C catalyst possesses a highly ordered porous matrix, which encompasses hierarchical micropores, mesopores, and macropores. This delicate porous structure markedly facilitates the mass transfer process of Fe sites and attains outstanding CO_2RR performance, particularly in the limited mass transfer region in the H-cell with a maximum CO current density of -19 mA cm^{-2}. SACs containing multiple metals have superior catalytic performance due to the common effect among adjacent single atoms. Wen *et al.*[93] developed a general and facile microwave-assisted rapid pyrolysis method to prepare carbon-based SACs with high porosity. Using a flow cell, it is measured that the single-atom nickel implanted nitrogen-doped carbon (Ni_1-N-C) derived from nickel-doped MOF (Ni-ZIF-8) shows remarkable CO FE (96%) and has a considerable CO partial current density of up to 1.06 A/cm^2 in CO_2 electroreduction, far superior to the counterpart obtained by traditional pyrolysis with electric heating, as shown in Figure 10F-H. Mechanism investigations reveal that the obtained Ni_1-N-C presents abundant defective sites and mesoporous structure, which greatly promotes the adsorption and mass transfer of CO_2. This work establishes a universal method for the rapid and large-scale synthesis of SACs and other carbon-based materials for efficient catalysis.

NRR

Ammonia (NH_3) is an important raw material chemical for the production of nitric acid, fertilizers, and explosives, and is also an essential component in many foods and fertilizers[94]. Currently, more than 90% of ammonia comes from the Haber-Bosch process, biological nitrogen fixation, and electrocatalysis. Although the Haber-Bosch process plays a role in biological nitrogen fixation, it often requires high temperature and pressure conditions. In addition, it has some drawbacks, including excessive dependence on the use of fossil fuels and the emission of large amounts of CO_2[95].

The reduction of nitrogen to ammonia on a non-homogeneous surface has two distinct mechanisms: dissociative and associative. In the dissociative mechanism, the N≡N bond is broken before hydrogenation, and individual nitrogen atoms are adsorbed on the catalyst surface and converted to NH_3 by hydrogenation. In the associative mechanism, when the nitrogen molecule is hydrogenated, the two nitrogen atoms remain bound to each other. There are two possible hydrogenation pathways: The first involves preferential hydrogenation occurring on the nitrogen atom furthest from the surface (assuming that the N_2 molecule is in terminal coordination mode). This pathway produces an equivalent of NH_3 while leaving an adsorbed nitrogen atom (or metal nitride M≡N unit) on the catalyst surface, which is subsequently hydrogenated to give a second equivalent of NH_3. The second pathway involves the individual hydrogenation of the nitrogen atoms in the two nitrogen centers until one of the nitrates is converted to NH_3 and the N≡N bond is broken.

Acidic condition:

Anode reaction:

$$3H_2O\ (l) \rightarrow 3/2O_2\ (g) + 6H^+\ (aq) + 6e^- \quad (25)$$

Cathode reaction:

$$N_2\ (g) + 6H^+\ (aq) + 6e^- \rightarrow 2NH_3\ (g) \quad (26)$$

Alkaline condition:

Anode reaction:

$$6OH^-\ (aq) \rightarrow 3H_2O\ (l) + 3/2O_2\ (g) + 6e^- \quad (27)$$

Cathode reaction:

$$N_2\ (g) + 6H_2O\ (l) + 6e^- \rightarrow 2NH_3\ (g) + 6OH^- \quad (28)$$

Starting with zirconium porphyrin MOF (PCN-222) as a precursor, a series of SACs (Fe_1-N-C, Co_1-N-C, Ni_1-N-C) were derived and constructed by varying the types of metals embedded in the porphyrin rings, and their electrocatalytic nitrogen reduction performance was studied[96]. As shown in Figure 11A-C, in the electrocatalytic nitrogen reduction test, Fe_1-N-C exhibited the best performance, with an ammonia production rate of 1.56 × 10^{-11} mol cm^{-2} s^{-1} at -0.05 V (*vs.* RHE), corresponding to a FE of 4.51%. The activity order of the three catalysts is: Fe_1-N-C > Co_1-N-C > Ni_1-N-C. The XANES of Fe_1-N-C indicates that the valence state of Fe is between that of Fe foil and Fe_2O_3 [Figure 11D]. The EXAFS results show that Fe is atomically dispersed in Fe_1-N-C in the form of Fe-N bonds, with no Fe-Fe bonds present [Figure 11E]. Further fitting suggests that Fe exists in the form of Fe-N_4. The existence of Fe SAs is also further confirmed by HAADF-STEM images [Figure 11F]. Additionally, by comparing SACs of the same substrate but different types, it can be observed that the change in the type of single-atom element has a significant impact on the performance of NRR. Therefore, the rational selection of the type of single atom can effectively enhance the catalytic performance and design high-performance electrocatalysts for nitrogen reduction. To better understand the capability of Fe_1-N-C for efficient NRR, the variation of ΔG along the NRR pathway at the zero-electrode potential (U = 0) was studied by DFT. The result exhibits that the NRR on Fe_1-N-C proceeds through the distal pathway, where N_2 adsorption is the RDS with a ΔG of 1.03 eV. In comparison, the RDS for both Co_1-N-C and Ni_1-N-C is the conversion from N_2^* to N_2H^*, with a ΔG of 1.30 eV and 2.29 eV, respectively, which is consistent with experimental catalytic performance and supports the high catalytic activity of Fe_1-N-C theoretically. To further investigate the difference of FE among these catalysts, Bader charge analysis was performed. The charge values of Fe, Co and Ni were +1.08 e, +0.87 e and +0.84 e, respectively. Considering the electrostatic repulsion between protons and positively charged metal atoms, the most positive charge on the Fe atom can prevent the approach of protons, significantly suppressing the HER process. With the lowest energy barrier of the RDS toward the NRR and the most sluggish HER kinetics, the best NRR performance of Fe_1-N-C can be well understood.

Due to the widespread presence of nitrates in industrial and domestic wastewater, electrocatalytic reduction of nitrates to synthesize ammonia is widely considered to be a promising methodological strategy. Compared to N_2, the bond energy of N=O in nitrates is only 204 kJ mol^{-1}, and nitrates have a higher solubility in aqueous solutions, making the Nitrate Reduction Reaction (NO_3RR) to ammonia more feasible than the reduction of nitrogen gas to ammonia. This also makes the application of NO_3RR easier to expand to other areas. However, the electrocatalytic reduction of nitrates is an eight-electron and nine-proton transfer process; thus, there is a high kinetic energy barrier for the reaction. How to carry out the NO_3RR process with high reactivity and energy conservation to efficiently synthesize ammonia is an urgent scientific question that needs to be addressed.

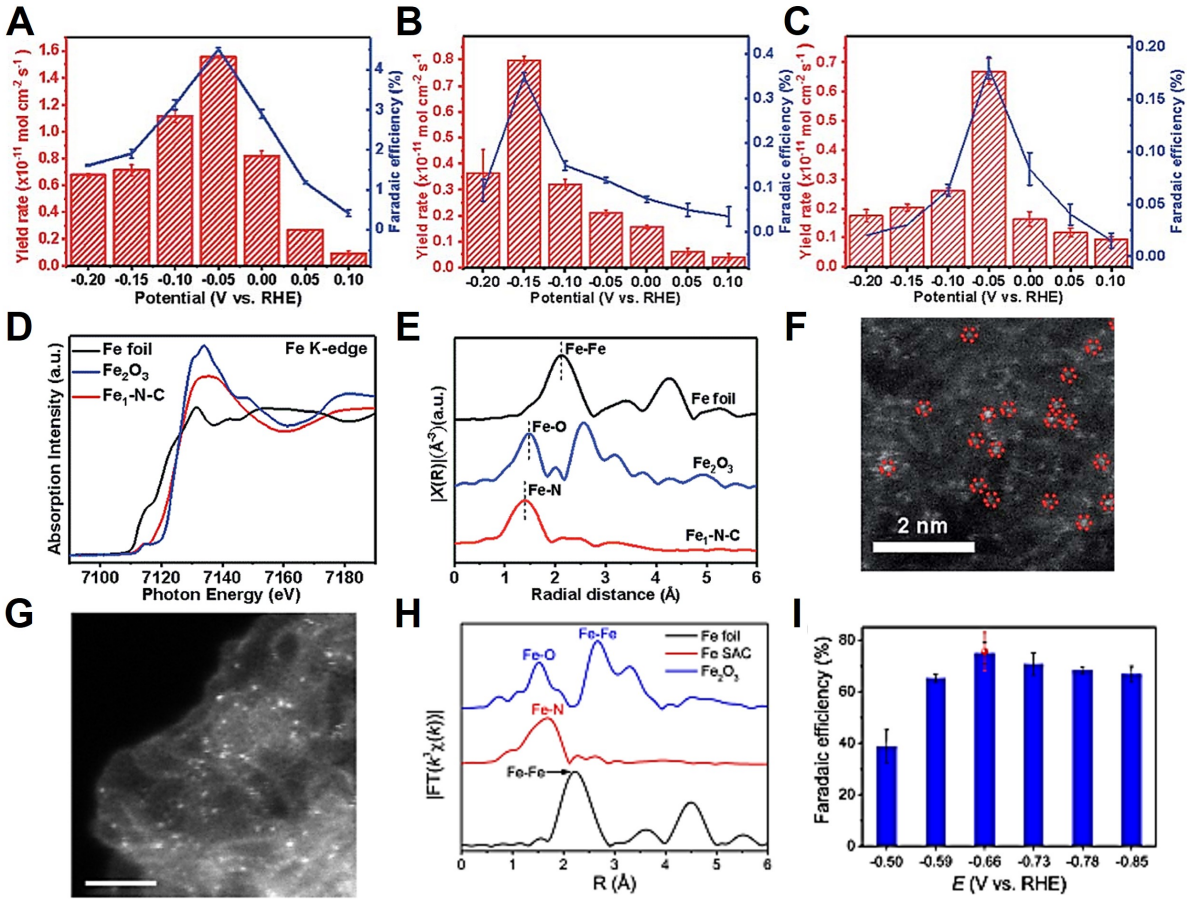

Figure 11. (A) NH_3 yield rate and FE of Fe_1-N-C at various potentials; NH_3 yield rate and FE of (B) Co_1-N-C and (C) Ni_1-N-C at various potentials; (D) Fe K-edge XANES; (E) FT-EXAFS curves of Fe foil, Fe_1-N-C and Fe_2O_3; (F) AC HAADF-STEM images of Fe_1-N-C. The (A-F) are quoted with permission from Zhang *et al.*[96]; (G) AC MAADF-STEM of Fe SAC; (H) FT k^3-weighted $\chi(k)$-function of the EXAFS spectra at Fe K-edge; (I) FE_{NH3} at each given potential. The (G-I) are quoted with permission from Wu *et al.*[97]. FE: Faradaic efficiency; FT-EXAFS: Fourier transform of extended X-ray absorption fine structure; AC HAADF-STEM: Aberration-corrected high-angle annular dark field scanning transmission electron microscopy; SACs: Single-atom catalysts.

Wu *et al.*[97] designed and prepared a Fe SAC with a lack of adjacent metal sites. In the AC HAADF-STEM images, Fe SAs supported on a nitrogen-containing carbon substrate can be clearly observed [Figure 11G]. The corresponding FT-EXAFS spectrum shows a characteristic peak near 1.6 Å, which belongs to the first shell of Fe-N coordination [Figure 11H]. Additionally, no Fe-Fe interaction peak is observed at 2.2 Å, thus indicating the absence of any Fe clusters or nanoparticles, and the Fe element exists in the form of a single atom. Fe atoms with N coordination but without adjacent metal coordination can effectively prevent the required N-N coupling step, thereby reducing the production ratio of intermediate products N_2H_2 and N_2H_4. This can improve the selectivity of ammonia products and effectively enhance the selectivity and activity of reducing nitrates to ammonia, with a maximum FE of approximately 75% [Figure 11I].

From the latest progress in SACs applied to NRR, Fe, Co, and Ni single-atom electrocatalysts can exhibit relatively good NRR catalytic activity and FE[98,99]. However, for large-scale industrial application and to achieve higher NH_3 yield and FE, further investigation of Fe, Co, and Ni SACs remains needed. This includes the rational selection and design of the corresponding substrate materials to enhance the intrinsic NRR activity of Fe, Co, and Ni SACs. Adjusting the structural characteristics of the carrier to better adapt to

the gas environment of NRR and ensure the full expression of the activity of Fe, Co, and Ni SAs. Properly regulating the adsorption energy of Fe, Co, and Ni to hydrogen to suppress the HER and ensure the effective progress of NRR.

Fe, Co, Ni SACs have many advantages in energy conversion, leading to their wide application. The applications of these catalysts in HER, OER, ORR, CO_2RR, NRR and NO_3RR fields are summarized here [Table 2].

CHALLENGES AND PERSPECTIVES

As a novel and highly efficient class of electrocatalysts, Fe, Co, and Ni SACs have demonstrated exceptional catalytic performance in various electrocatalytic reactions. By optimizing the catalyst preparation methods and the properties of support materials, the activity and stability of these catalysts can be further enhanced. The extensive application of Fe, Co, and Ni SACs will provide robust support for the development of energy conversion and storage technologies. Despite the significant progress made in the field of Fe, Co, and Ni SACs for electrocatalysis, several challenges and issues remain to be addressed:

Synthesis challenges: The synthesis of Fe, Co, and Ni SACs confronts numerous hurdles, primarily stemming from stringent requirements in technology, equipment, and operational conditions to ensure the high dispersion of metal atoms on the support. This high dispersion is crucial for optimizing the performance of Fe, Co, and Ni SACs; however, it also raises significant issues related to scalability and reproducibility of the synthesis process. Pursuing high SACs loading rates necessitates maintaining metal atom stability, which poses another major challenge. High-temperature calcination is often employed to strengthen the bonding between metal single atoms and anchoring sites, yet this process carries the risk of metal atom aggregation, potentially leading to a significant decrease in atom utilization and catalytic performance. Although subsequent acid washing can remove some metal aggregates, it undoubtedly complicates the synthesis steps, prolongs the preparation cycle, and may adversely affect the final metal loading rate. Future research on Fe, Co, and Ni SACs should focus on further optimizing preparation methods, aiming to achieve both high dispersion and stable anchoring of metal atoms. This necessitates continuous exploration and innovation in support design, anchoring site selection and control, fine-tuning of calcination conditions, and simplification of post-treatment processes to overcome the limitations of existing technologies.

Stability under harsh conditions: The deactivation and structural changes of Fe, Co, and Ni SACs under extreme catalytic conditions, such as high temperature, high pressure, and corrosive environments, are crucial factors limiting their industrial applications. To ensure the widespread applicability of Fe, Co, and Ni SACs, it is vital to delve into their deactivation mechanisms under harsh working conditions. While some Fe, Co, and Ni SACs can meet commercial standards under laboratory conditions, their insufficient stability in practical applications remains a major obstacle to be addressed. Single metal sites, due to their high surface energy, tend to spontaneously form thermally stable metal clusters during catalysis, leading to structural instability of Fe, Co, and Ni SACs. Furthermore, the complexity of working conditions, including acid-base electrolytes, fluctuations in redox potentials, and the presence of harmful radicals, can weaken or disrupt the contact between the support and metal sites, promoting the dissolution or aggregation of single metal sites and thereby accelerating deactivation of SACs. For carbon-based SACs, while high graphitization levels can significantly enhance corrosion resistance and catalytic stability, they also lead to a decrease in active site density. Therefore, maintaining or enhancing active site density while preserving high stability is crucial to overcoming the activity-stability trade-off. Future research should focus on deeply understanding the deactivation mechanisms of Fe, Co, and Ni SACs under extreme conditions and comprehensively

Table 2. Summary of synthesis methods and main performances of Fe, Co, Ni SACs for HER, OER, ORR, CO_2RR, NRR, and NO_3RR

Materials	Synthesis methods	Electrocatalysis reaction	Electrolytes	Performance metrics		Refs.
C-Co-MoS_2	High-temperature pyrolysis	HER	Acid	Overpotential: 17 mV (10 mA/cm^2)	Tafel slope: 32 mV/dec	[73]
Co-SAC/RuO_2	High-temperature pyrolysis	HER	0.5 M H_2SO_4	Overpotential: 45 mV (10 mA/cm^2)	Tafel slope: 58 mV/dec	[29]
Fe-SAC@COF	Impregnation	OER	1 M KOH	Overpotential: 290 mV (10 mA/cm^2)	Tafel slope: 40 mV/dec	[66]
CoMM	High-temperature pyrolysis	OER	1 M KOH	Overpotential: 351 mV (10 mA/cm^2)	Tafel slope: 84 mV/dec	[77]
Ni SAs@S/N-FCS	CVD	OER	1 M KOH	Overpotential: 249 mV (10 mA/cm^2)	Tafel slope: 56.5 mV/dec	[61]
Ni_{SA}-O/Mo_2C	High-temperature pyrolysis	OER	1 M KOH	Overpotential: 299 mV (10 mA/cm^2)	Tafel slope: 89.36 mV/dec	[72]
Fe SAC/N-C	High-temperature pyrolysis	ORR	0.1 M KOH	Half-wave: 0.89 V *vs.* RHE	-	[66]
ISAS-Co/HNCS	High-temperature pyrolysis	ORR	0.5 M H_2SO_4	Half-wave: 0.773 V *vs.* RHE	Tafel slope: 34 mV/dec	[81]
Ni SAs-NC	High-temperature pyrolysis	ORR	0.1 M KOH	Half-wave: 0.85 V *vs.* RHE	Tafel slope: 56 mV/dec	[82]
Ni-NC(HPU)	High-temperature pyrolysis	CO_2RR	0.5 M $KHCO_3$	FE_{CO}: 91% (-0.8 V *vs.* RHE)	J_{CO}: -24.7 mA/cm^2 (-0.8 V *vs.* RHE)	[43]
Fe-S_1N_3	High-temperature pyrolysis	CO_2RR	0.5 M $KHCO_3$	FE_{CO}: 99.02% (-0.5 V *vs.* RHE)	J_{CO}: -77.15 ± 4.46 mA/cm^2 (-1.2 V *vs.* RHE)	[52]
Fe_1-N-C	High-temperature pyrolysis	NRR	0.1 M HCl	Potential: -0.05 V *vs.* RHE	NH_3 yield: 1.56 × 10^{-11} mol/cm·s	[96]
Fe-SAs/LCC	High-temperature pyrolysis	NRR	0.1 M KOH	Potential: -0.1 V *vs.* RHE	NH_3 yield: 32.1 μg/h·mg$_{cat}$	[100]
FeNP/NC	Impregnation	NO_3RR	0.1 M K_2SO_4 + 0.5 M KNO_3	Potential: -0.85 V *vs.* RHE	NH_3 yield: ~20,000 μg/h·mg$_{cat}$	[97]
Fe-N/P-C	High-temperature pyrolysis	NO_3RR	0.1 M KOH + 0.1 M KNO_3	Potential: -0.8 V *vs.* RHE	NH_3 yield: 17,980 μg/h·mg$_{cat}$	[101]

HER: Hydrogen evolution reaction; CoMM: Graphenic network using melem; ORR: Oxygen reduction reaction; NRR: Nitrogen reduction reaction; SACs: Single-atom catalysts; OER: Oxygen evolution reaction; CO_2RR: Carbon dioxide reduction reaction; NO_3RR: Nitrate Reduction Reaction; SAs: Single atoms; RHE: Reversible hydrogen electrode; ISAS: Isolated single-atom sites; CVD: Chemical vapor deposition.

enhancing their catalytic stability and activity through optimized support design, precise defect control, and the introduction of stable metal components, to meet the stringent requirements of industrial applications.

Limitations in Characterization Conditions: The characterization of Fe, Co, and Ni SACs faces inherent challenges stemming from their minute sizes and low metal loadings. Traditional microscopy tools are limited by resolution and struggle to directly observe individual atoms. Modern microscopy techniques, such as aberration-corrected TEM and STM, have been introduced, but they too face challenges related to sample preparation difficulty and catalyst stability under operating conditions. Accurately deciphering atomic structures of Fe, Co, and Ni SACs is crucial for understanding their catalytic functions. Spectroscopic techniques, such as XAS and EXAFS, provide powerful tools to reveal the coordination environment and local atomic structure of metal single atoms. However, distinguishing individual atoms from tiny metal clusters remains subtle and complex, and the dynamic changes in structures of Fe, Co, and Ni SACs during catalysis further complicate this task. The dynamic nature of Fe, Co, and Ni SACs, where atoms migrate and reorganize during catalytic reactions, adds difficulty to capturing and identifying reaction intermediates and transient species. Techniques such as in situ spectroscopy, operando characterization, and time-resolved spectroscopy have emerged to monitor these dynamic changes

intuitively. While these techniques offer real-time, dynamic information on catalytic processes, they often require complex experimental setups and high technical expertise, raising the research threshold. The characterization of Fe, Co, and Ni SACs necessitates a multi-faceted approach leveraging advanced technologies to overcome the challenges posed by material properties and experimental conditions, comprehensively and precisely revealing their catalytic mechanisms and dynamic behaviors, thereby laying a solid foundation for the further optimization and widespread application of these SACs.

Limited Understanding of Reaction Mechanisms: Exploring the reaction mechanisms of Fe, Co, and Ni SACs presents multiple challenges. Firstly, the unique structures and properties of these SACs suggest that their catalytic mechanisms may significantly differ from those of traditional bulk metal catalysts, complicating the understanding and prediction of their catalytic behaviors. Fe, Co, and Ni SACs often generate short-lived, highly reactive intermediates during catalysis, which are difficult to identify and characterize experimentally, severely hindering our clear understanding of complete reaction pathways. Secondly, the diverse coordination and structural environments of Fe, Co, and Ni SACs, governed by metal atoms and their supporting substrates, make exploring the specific impacts of different atomic structures on catalytic activity and selectivity exceedingly complex. This requires interdisciplinary research methods integrating sophisticated experimental techniques and in-depth theoretical analyses. In computational modeling, tools such as DFT are crucial for unraveling the reaction mechanisms of Fe, Co, and Ni SACs. However, accurately predicting the behaviors of individual atoms under complex catalytic reaction conditions remains a formidable task.

Fe, Co, Ni SACs present some unique challenges. First of all, in terms of cost, Fe, Co, Ni and other metals have lower prices than precious metals (such as Pt, Au, Pd, *etc.*), and have cost advantages in large-scale applications. However, its preparation process is generally more complicated. If special synthesis methods or conditions are required, the preparation cost will be increased. In some cases, the total cost may not be low. Secondly, in terms of catalytic activity, the catalytic active site properties of Fe, Co, Ni and other metals are different from those of precious metals, and the catalytic activity for specific reactions may not be as high as that of precious metal SACs. For example, in some fine chemical or high-end material preparation fields that require very high catalytic activity, the advantages of precious metal SACs may be more obvious. However, through reasonable design and regulation, such as optimizing the coordination environment and carrier properties of metals, Fe, Co, Ni SACs can also show better catalytic activity. They may have unique catalytic properties and selectivity in some specific reactions, such as those involving the formation or breaking of C-O and C-N bonds. Finally, in terms of stability, Fe, Co, and Ni may be more prone to oxidation, corrosion and other phenomena in some environments, affecting the stability and service life of the catalyst. For instance, in oxidizing atmospheres or in reaction systems where certain corrosive substances are present, Fe, Co, Ni SACs may require special protective measures or carrier optimization to improve stability. In addition, the interaction between these metal single atoms and the carrier is relatively weak, and aggregation or migration of single atoms may occur during the reaction, resulting in catalyst deactivation.

CONCLUSIONS

In summary, Fe, Co and Ni are abundant transition metal elements, which are cheaper and easier to obtain than precious metals (such as Pt, Pd, *etc.*). Therefore, Fe, Co, and Ni SACs exhibit tremendous application potential and development prospects in the field of electrocatalysis. However, the current synthesis of these SAC catalysts faces challenges. Firstly, synthesizing these catalysts efficiently with highly dispersed and stably anchored metal atoms poses technological, equipment, and operational hurdles, necessitating the refinement of existing synthesis methods. Secondly, under rigorous catalytic conditions, Fe, Co, and Ni

SACs are susceptible to deactivation, highlighting the importance of studying deactivation mechanisms and enhancing their stability. Furthermore, the minute scale of these materials limits characterization efforts, demanding the integrated use of advanced technologies for precise atomic-scale analysis. Lastly, the intricacies of catalytic reaction mechanisms underscore the need for interdisciplinary research to unravel microscopic processes and optimize SAC performance. To propel their widespread adoption in clean energy technologies, future research must focus on refining preparation methodologies, elucidating stability mechanisms, deeply probing catalytic pathways, and addressing industrialization challenges.

DECLARATIONS

Authors' contributions

Wrote the manuscript and designed the figures: Yang, Y.; Huang, M.; Wang, C.; Wu, H.; Yuan, Y.; Zheng, J.
Organized the references: Yang, Y.; Huang, M.; Wang, C.; Wu, H.; Yuan, Y.; Zheng, J.
Revised the manuscript: Yang, Y.; Gao, B.; Huang, M.; Wang, C.; Wu, H.; Yuan, Y.
Supervised the whole study and structured and revised the manuscript: Zheng, J.

Availability of data and materials

Data will be made available on request.

Financial support and sponsorship

This work was financially supported by the National Natural Science Foundation of China (52271200), Guangdong Basic and Applied Basic Research Foundation (2024A1515010393), and the Fundamental Research Funds for the Central Universities (FRF-TP-18-079A1).

Conflicts of interest

All authors declared that there are no conflicts of interest.

Ethical approval and consent to participate

Not applicable.

Consent for publication

Not applicable.

REFERENCES

1. Zhou, A.; Wang, D.; Li, Y. Hollow microstructural regulation of single-atom catalysts for optimized electrocatalytic performance. *Microstructures* **2022**, *2*, 2022005. DOI
2. Kendall, M. Fuel cell development for new energy vehicles (NEVs) and clean air in China. *Prog. Nat. Sci. Mater. Int.* **2018**, *28*, 113-20. DOI
3. Tarhan, C.; Çil, M. A. A study on hydrogen, the clean energy of the future: hydrogen storage methods. *J. Energy. Storage.* **2021**, *40*, 102676. DOI
4. Zhao, Y.; Adiyeri, S. D. P.; Huang, C.; et al. Oxygen evolution/reduction reaction catalysts: from in situ monitoring and reaction mechanisms to rational design. *Chem. Rev.* **2023**, *123*, 6257-358. DOI
5. Wu, K.; Lyu, C.; Cheng, J.; et al. Defect engineering in transition-metal (Fe, Co, and Ni)-based electrocatalysts for water splitting. *Carbon. Energy.* **2024**, *6*, e485. DOI
6. Verma, J.; Goel, S. Cost-effective electrocatalysts for hydrogen evolution reactions (HER): challenges and prospects. *Int. J. Hydrogen. Energy.* **2022**, *47*, 38964-82. DOI
7. Jin, S.; Hao, Z.; Zhang, K.; Yan, Z.; Chen, J. Advances and challenges for the electrochemical reduction of CO_2 to CO: from fundamentals to industrialization. *Angew. Chem. Int. Ed.* **2021**, *133*, 20795-816. DOI
8. Qing, G.; Ghazfar, R.; Jackowski, S. T.; et al. Recent advances and challenges of electrocatalytic N_2 reduction to ammonia. *Chem.*

Rev. **2020**, *120*, 5437-516. DOI
9. Zhang, Y.; Lin, Y.; Duan, T.; Song, L. Interfacial engineering of heterogeneous catalysts for electrocatalysis. *Mater. Today.* **2021**, *48*, 115-34. DOI
10. Long, X.; Li, Z.; Gao, G.; et al. Graphitic phosphorus coordinated single Fe atoms for hydrogenative transformations. *Nat. Commun.* **2020**, *11*, 4074. DOI PubMed PMC
11. Wu, T.; Han, M. Y.; Xu, Z. J. Size effects of electrocatalysts: more than a variation of surface area. *ACS. Nano.* **2022**, *16*, 8531-9. DOI
12. Wang, H.; Lu, J. A review on particle size effect in metal-catalyzed heterogeneous reactions. *Chin. J. Chem.* **2020**, *38*, 1422-44. DOI
13. Yu, X.; Li, G.; Tao, S.; et al. Single-atom Fe catalyst for catalytic ethane dehydrogenation to ethylene. *ChemCatChem* **2023**, *15*, e202201612. DOI
14. Tong, M.; Sun, F.; Xing, G.; Tian, C.; Wang, L.; Fu, H. Potential dominates structural recombination of single atom Mn sites for promoting oxygen reduction reaction. *Angew. Chem. Int. Ed.* **2023**, *62*, e202314933. DOI
15. Jia, C.; Li, S.; Zhao, Y.; et al. Nitrogen vacancy induced coordinative reconstruction of single-atom Ni catalyst for efficient electrochemical CO_2 reduction. *Adv. Funct. Materials.* **2021**, *31*, 2107072. DOI
16. Xu, H.; Cheng, D.; Cao, D.; Zeng, X. C. Revisiting the universal principle for the rational design of single-atom electrocatalysts. *Nat. Catal.* **2024**, *7*, 207-18. DOI
17. Wu, X.; Zhang, H.; Zuo, S.; et al. Engineering the coordination sphere of isolated active sites to explore the intrinsic activity in single-atom catalysts. *Nanomicro. Lett.* **2021**, *13*, 136. DOI PubMed PMC
18. Liu, H.; Tian, L.; Zhang, Z.; et al. Atomic-level asymmetric tuning of the Co_1-N_3P_1 catalyst for highly efficient *N*-alkylation of amines with alcohols. *J. Am. Chem. Soc.* **2024**, *146*, 20518-29. DOI
19. Deng, Z.; Liu, Y.; Lin, J.; Chen, W. Rational design and energy catalytic application of high-loading single-atom catalysts. *Rare. Met.* **2024**, *43*, 4844-66. DOI
20. Guo, W.; Wang, Z.; Wang, X.; Wu, Y. General design concept for single-atom catalysts toward heterogeneous catalysis. *Adv. Mater.* **2021**, *33*, e2004287. DOI
21. Liang, J.; Lin, J.; Yang, X.; et al. Theoretical and experimental investigations on single-atom catalysis: Ir_1/FeO*x* for CO oxidation. *J. Phys. Chem. C.* **2014**, *118*, 21945-51. DOI
22. Tian, J.; Zhu, Y.; Yao, X.; et al. Chemical vapor deposition towards atomically dispersed iron catalysts for efficient oxygen reduction. *J. Mater. Chem. A.* **2023**, *11*, 5288-95. DOI
23. Yan, H.; Zhang, N.; Wang, D. Highly efficient CeO_2-supported noble-metal catalysts: from single atoms to nanoclusters. *Chem. Catalysis.* **2022**, *2*, 1594-623. DOI
24. Park, S. J.; Nguyen, T. H.; Tran, D. T.; Dinh, V. A.; Lee, J. H.; Kim, N. H. Delaminated MBene sheets beyond usual 2D transition metal materials for securing Pt single atoms to boost hydrogen evolution. *Energy. Environ. Sci.* **2023**, *16*, 4093-104. DOI
25. Tan, H.; Wang, J.; Lin, S.; Kuo, T.; Chen, H. M. Dynamic coordination structure evolutions of atomically dispersed metal catalysts for electrocatalytic reactions. *Adv. Mater. Inter.* **2023**, *10*, 2202050. DOI
26. Liu, Y.; Zhuang, Z.; Liu, Y.; et al. Shear-strained Pd single-atom electrocatalysts for nitrate reduction to ammonia. *Angew. Chem. Int. Ed.* **2024**, *63*, e202411396. DOI
27. Zhu, Y.; Wang, J.; Koketsu, T.; et al. Author correction: iridium single atoms incorporated in Co_3O_4 efficiently catalyze the oxygen evolution in acidic conditions. *Nat. Commun.* **2024**, *15*, 1395. DOI PubMed PMC
28. Mochizuki, C.; Inomata, Y.; Yasumura, S.; et al. Defective NiO as a stabilizer for Au single-atom catalysts. *ACS. Catal.* **2022**, *12*, 6149-58. DOI
29. Shah, K.; Dai, R.; Mateen, M.; et al. Cobalt single atom incorporated in ruthenium oxide sphere: a robust bifunctional electrocatalyst for HER and OER. *Angew. Chem.* **2022**, *61*, e202114951. DOI
30. Wang, Y.; Shi, R.; Shang, L.; et al. High-efficiency oxygen reduction to hydrogen peroxide catalyzed by nickel single-atom catalysts with tetradentate N_2O_2 coordination in a three-phase flow cell. *Angew. Chem. Int. Ed.* **2020**, *59*, 13057-62. DOI
31. Mosrati, J.; Abdel-mageed, A. M.; Vuong, T. H.; et al. Tiny species with big impact: high activity of Cu single atoms on CeO_2-TiO_2 deciphered by operando spectroscopy. *ACS. Catal.* **2021**, *11*, 10933-49. DOI
32. Wu, Y.; Zhao, Y.; Zhai, P.; et al. Triggering lattice oxygen activation of single-atomic Mo sites anchored on Ni-Fe oxyhydroxides nanoarrays for electrochemical water oxidation. *Adv. Mater.* **2022**, *34*, e2202523. DOI
33. Zheng, Y.; Li, S.; Huang, N.; Li, X.; Xu, Q. Recent advances in metal-organic framework-derived materials for electrocatalytic and photocatalytic CO_2 reduction. *Coord. Chem. Rev.* **2024**, *510*, 215858. DOI
34. Gloag, L.; Somerville, S. V.; Gooding, J. J.; Tilley, R. D. Co-catalytic metal-support interactions in single-atom electrocatalysts. *Nat. Rev. Mater.* **2024**, *9*, 173-89. DOI
35. Chen, Z.; Li, X.; Zhao, J.; et al. Stabilizing Pt single atoms through Pt-Se electron bridges on vacancy-enriched nickel selenide for efficient electrocatalytic hydrogen evolution. *Angew. Chem. Int. Ed.* **2023**, *62*, e202308686. DOI
36. Jia, C.; Zhao, Y.; Song, S.; et al. Highly ordered hierarchical porous single-atom Fe catalyst with promoted mass transfer for efficient electroreduction of CO_2. *Adv. Energy. Mater.* **2023**, *13*, 2302007. DOI
37. Liu, J.; Cao, C.; Liu, X.; et al. Direct observation of metal oxide nanoparticles being transformed into metal single atoms with oxygen-coordinated structure and high-loadings. *Angew. Chem. Int. Ed.* **2021**, *60*, 15248-53. DOI
38. Zhou, Y.; Song, E.; Chen, W.; et al. Dual-metal interbonding as the chemical facilitator for single-atom dispersions. *Adv. Mater.*

2020, *32*, e2003484. DOI

39. Wang, M.; Yang, W.; Li, X.; et al. Atomically dispersed Fe-heteroatom (N, S) bridge sites anchored on carbon nanosheets for promoting oxygen reduction reaction. *ACS. Energy. Lett.* **2021**, *6*, 379-86. DOI
40. Hao, Y.; Hung, S. F.; Zeng, W. J.; et al. Switching the oxygen evolution mechanism on atomically dispersed Ru for enhanced acidic reaction kinetics. *J. Am. Chem. Soc.* **2023**, *145*, 23659-69. DOI
41. Zhao, L.; Bian, J.; Zhang, X.; et al. Construction of ultrathin s-scheme heterojunctions of single Ni atom immobilized Ti-MOF and $BiVO_4$ for CO_2 photoconversion of nearly 100% to CO by pure water. *Adv. Mater.* **2022**, *34*, e2205303. DOI
42. Cheng, Y.; Peng, J.; Lai, G.; et al. Edge-site Co-N*x* model single-atom catalysts for CO_2 electroreduction. *ACS. Catal.* **2024**, *14*, 8446-55. DOI
43. Li, Y.; Lu, X. F.; Xi, S.; Luan, D.; Wang, X.; Lou, X. W. D. Synthesis of N-doped highly graphitic carbon urchin-like hollow structures loaded with single-Ni atoms towards efficient CO_2 electroreduction. *Angew. Chem. Int. Ed.* **2022**, *61*, e202201491. DOI
44. Li, B. Q.; Zhao, C. X.; Chen, S.; et al. Framework-porphyrin-derived single-atom bifunctional oxygen electrocatalysts and their applications in Zn-air batteries. *Adv. Mater.* **2019**, *31*, e1900592. DOI
45. Li, Q.; Chen, W.; Xiao, H.; et al. Fe isolated single atoms on S, N codoped carbon by copolymer pyrolysis strategy for highly efficient oxygen reduction reaction. *Adv. Mater.* **2018**, *30*, e1800588. DOI
46. Lim, J. W.; Choo, D. H.; Cho, J. H.; et al. A MOF-derived pyrrolic N-stabilized Ni single atom catalyst for selective electrochemical reduction of CO_2 to CO at high current density. *J. Mater. Chem. A.* **2024**, *12*, 11090-100. DOI
47. Yang, H.; Zhang, P.; Yi, X.; et al. Constructing highly utilizable Fe-N_4 single-atom sites by one-step gradient pyrolysis for electroreduction of O_2 and CO_2. *Chem. Eng. J.* **2022**, *440*, 135749. DOI
48. Pan, Y.; Chen, Y.; Wu, K.; et al. Regulating the coordination structure of single-atom Fe-N_xC_y catalytic sites for benzene oxidation. *Nat. Commun.* **2019**, *10*, 4290. DOI PubMed PMC
49. Koshy, D. M.; Chen, S.; Lee, D. U.; et al. Understanding the origin of highly selective CO_2 electroreduction to CO on Ni,N-doped carbon catalysts. *Angew. Chem. Int. Ed.* **2020**, *59*, 4043-50. DOI
50. Lei, J.; Liu, H.; Yin, D.; et al. Boosting the loading of metal single atoms via a bioconcentration strategy. *Small* **2020**, *16*, e1905920. DOI
51. Wei, S.; Yang, R.; Zhang, Q. Isolated iron single-atom sites for oxygen reduction derived from a porphyrin-based carbon sphere by a polymerization-coordination-pyrolysis strategy. *J. Mater. Chem. A.* **2023**, *11*, 16314-20. DOI
52. Wang, J.; Huang, Y.; Wang, Y.; et al. Atomically dispersed metal-nitrogen-carbon catalysts with *d*-orbital electronic configuration-dependent selectivity for electrochemical CO_2-to-CO reduction. *ACS. Catal.* **2023**, *13*, 2374-85. DOI
53. Noh, W. Y.; Mun, J.; Lee, Y.; et al. Molecularly engineered carbon platform to anchor edge-hosted single-atomic M-N/C (M = Fe, Co, Ni, Cu) electrocatalysts of outstanding durability. *ACS. Catal.* **2022**, *12*, 7994-8006. DOI
54. Xu, H.; Zhang, S.; Zhang, X.; et al. Atomically dispersed iron regulating electronic structure of iron atom clusters for electrocatalytic H_2O_2 Production and biomass upgrading. *Angew. Chem. Int. Ed.* **2023**, *62*, e202314414. DOI
55. Shi, B.; Li, H.; Fu, X.; et al. Fe Single-atom catalyst for cost-effective yet highly efficient heterogeneous fenton catalysis. *ACS. Appl. Mater. Interfaces.* **2022**, *14*, 53767-76. DOI
56. Tan, H.; Tang, J.; Henzie, J.; et al. Assembly of hollow carbon nanospheres on graphene nanosheets and greation of iron-nitrogen-doped porous carbon for oxygen reduction. *ACS. Nano.* **2018**, *12*, 5674-83. DOI
57. Min, S.; Wang, Z.; Xu, X.; et al. Transition metal (Fe, Co, Ni)-doped cuprous oxide nanowire arrays as self-supporting catalysts for electrocatalytic CO_2 reduction reaction to ethylene. *Appl. Surf. Sci.* **2024**, *663*, 160150. DOI
58. Wang, J.; Li, B.; Li, Y.; et al. Facile synthesis of atomic Fe-N-C materials and dual roles investigation of Fe-N_4 sites in fenton-like reactions. *Adv. Sci.* **2021**, *8*, e2101824. DOI
59. Yin, S.; Yang, S.; Li, G.; et al. Seizing gaseous Fe^{2+} to densify O_2-accessible Fe-N_4 sites for high-performance proton exchange membrane fuel cells. *Energy. Environ. Sci.* **2022**, *15*, 3033-40. DOI
60. Yuan, S.; Zhang, J.; Hu, L.; et al. Decarboxylation-induced defects in MOF-derived single cobalt atom@carbon electrocatalysts for efficient oxygen reduction. *Angew. Chem. Int. Ed.* **2021**, *60*, 21685-90. DOI
61. Zhao, Y.; Lu, X. F.; Fan, G.; Luan, D.; Gu, X.; Lou, X. W. D. Surface-exposed single-Ni atoms with potential-driven dynamic behaviors for highly efficient electrocatalytic oxygen evolution. *Angew. Chem. Int. Ed.* **2022**, *61*, e202212542. DOI
62. Wang, C.; Tissot, H.; Soldemo, M.; Lu, J.; Weissenrieder, J. Inverse single-site $Fe_1(OH)_x$/Pt(111) model catalyst for preferential oxidation of CO in H_2. *Nano. Res.* **2022**, *15*, 709-15. DOI
63. Chaipornchalerm, P.; Nunthakitgoson, W.; Mano, P.; et al. Rational design of Fe single sites supported on hierarchical zeolites via atomic layer deposition for few-walled carbon nanotube production. *ACS. Appl. Mater. Interfaces.* **2024**, *16*, 33590-600. DOI
64. Zhang, L.; Wang, Q.; Li, L.; et al. Single atom surface engineering: a new strategy to boost electrochemical activities of Pt catalysts. *Nano. Energy.* **2022**, *93*, 106813. DOI
65. Cao, Y.; Chen, S.; Luo, Q.; et al. Atomic-level insight into optimizing the hydrogen evolution pathway over a Co_1-N_4 single-site photocatalyst. *Angew. Chem. Int. Ed.* **2017**, *56*, 12191-6. DOI
66. Wang, X.; Sun, L.; Zhou, W.; et al. Iron single-atom catalysts confined in covalent organic frameworks for efficient oxygen evolution reaction. *Cell. Rep. Phys. Sci.* **2022**, *3*, 100804. DOI
67. Wang, X.; Jin, B.; Jin, Y.; Wu, T.; Ma, L.; Liang, X. Supported single Fe atoms prepared via atomic layer deposition for catalytic reactions. *ACS. Appl. Nano. Mater.* **2020**, *3*, 2867-74. DOI

68. Yan, H.; Zhao, X.; Guo, N.; et al. Atomic engineering of high-density isolated Co atoms on graphene with proximal-atom controlled reaction selectivity. *Nat. Commun.* **2018**, *9*, 3197. DOI PubMed PMC
69. Bu, F.; Chen, C.; Yu, Y.; et al. Boosting benzene oxidation with a spin-state-controlled nuclearity effect on iron sub-nanocatalysts. *Angew. Chem.* **2023**, *62*, e202216062. DOI
70. Jin, T.; Liu, X.; Gao, Q.; et al. Pyrolysis-free, facile mechanochemical strategy toward cobalt single-atom/nitrogen-doped carbon for highly efficient water splitting. *Chem. Eng. J.* **2022**, *433*, 134089. DOI
71. Zhao, X.; Zheng, X.; Lu, Q.; et al. Electrocatalytic enhancement mechanism of cobalt single atoms anchored on different MXene substrates in oxygen and hydrogen evolution reactions. *EcoMat* **2023**, *5*, e12293. DOI
72. Yang, H.; Lin, Q.; Zhang, C.; et al. Carbon dioxide electroreduction on single-atom nickel decorated carbon membranes with industry compatible current densities. *Nat. Commun.* **2020**, *11*, 593. DOI PubMed PMC
73. Gong, F.; Liu, Y.; Zhao, Y.; et al. Back cover: universal sub-nanoreactor strategy for synthesis of yolk-shell MoS_2 supported single atom electrocatalysts toward robust hydrogen evolution reaction. *Angew. Chem. Int. Ed.* **2023**, *62*, e202308091. DOI
74. Liu, J. C.; Wang, Y. G.; Li, J. Toward rational design of oxide-supported single-atom catalysts: atomic dispersion of gold on ceria. *J. Am. Chem. Soc.* **2017**, *139*, 6190-9. DOI
75. Lin, L.; Zhou, W.; Gao, R.; et al. Low-temperature hydrogen production from water and methanol using Pt/α-MoC catalysts. *Nature* **2017**, *544*, 80-3. DOI
76. Zhao, Y.; Guo, Y.; Lu, X. F.; Luan, D.; Gu, X.; Lou, X. W. D. Exposing single Ni atoms in hollow S/N-doped carbon macroporous fibers for highly efficient electrochemical oxygen evolution. *Adv. Mater.* **2022**, *34*, e2203442. DOI
77. Kumar, P.; Kannimuthu, K.; Zeraati, A. S.; et al. High-density cobalt single-atom catalysts for enhanced oxygen evolution reaction. *J. Am. Chem. Soc.* **2023**, *145*, 8052-63. DOI
78. Hou, M.; Zheng, L.; Zhao, D.; et al. Microenvironment reconstitution of highly active Ni single atoms on oxygen-incorporated Mo_2C for water splitting. *Nat. Commun.* **2024**, *15*, 1342. DOI PubMed PMC
79. Jasinski, R. A new fuel cell cathode catalyst. *Nature* **1964**, *201*, 1212-3. DOI
80. Lin, Y.; Liu, P.; Velasco, E.; et al. Fabricating single-atom catalysts from chelating metal in open frameworks. *Adv. Mater.* **2019**, *31*, e1808193. DOI
81. Han, Y.; Wang, Y. G.; Chen, W.; et al. Hollow N-doped carbon spheres with isolated cobalt single atomic sites: superior electrocatalysts for oxygen reduction. *J. Am. Chem. Soc.* **2017**, *139*, 17269-72. DOI
82. Jiang, H.; Xia, J.; Jiao, L.; et al. Ni single atoms anchored on N-doped carbon nanosheets as bifunctional electrocatalysts for urea-assisted rechargeable Zn-air batteries. *Appl. Catal. B:. Environ.* **2022**, *310*, 121352. DOI
83. Wroblowa, H. S.; Yen-chi-pan; Razumney, G. Electroreduction of oxygen: a new mechanistic criterion. *J. Electroanal. Chem. Interfacial. Electrochem.* **1976**, *69*, 195-201. DOI
84. Ye, C.; Xu, L. Recent advances in the design of a high performance metal-nitrogen-carbon catalyst for the oxygen reduction reaction. *J. Mater. Chem. A.* **2021**, *9*, 22218-47. DOI
85. Kang, Z.; Wang, X.; Wang, D.; et al. Carbon-based single-atom catalysts: impacts of atomic coordination on the oxygen reduction reaction. *Nanoscale* **2023**, *15*, 9605-34. DOI
86. Jun S, Choi S, Kim J, Kwon KC, Park SH, Jang HW. Non-noble metal single atom catalysts for electrochemical energy conversion reactions. *Chinese. J. Catal.* **2023**, *50*, 195-214. DOI
87. Liang, Z.; Zheng, H.; Cao, R. Recent advances in Co-based electrocatalysts for the oxygen reduction reaction. *Sustain. Energy. Fuels.* **2020**, *4*, 3848-70. DOI
88. Garba, M. D.; Usman, M.; Khan, S.; et al. CO_2 towards fuels: a review of catalytic conversion of carbon dioxide to hydrocarbons. *J. Environ. Chem. Eng.* **2021**, *9*, 104756. DOI
89. Goyal, N.; Li, F.; Hu, Y. Tailoring single-metal atom catalysts: a strategic defect engineering approach for electrochemical reduction reactions. *J. Mater. Chem. A.* **2024**, *12*, 19685-719. DOI
90. Tang, T.; Wang, Z.; Guan, J. Optimizing the electrocatalytic selectivity of carbon dioxide reduction reaction by regulating the electronic structure of single-atom M-N-C materials. *Adv. Funct. Mater.* **2022**, *32*, 2111504. DOI
91. Pei, J.; Shang, H.; Mao, J.; et al. A replacement strategy for regulating local environment of single-atom Co-S_xN_{4-x} catalysts to facilitate CO_2 electroreduction. *Nat. Commun.* **2024**, *15*, 416. DOI
92. Chen, S.; Li, X.; Kao, C. W.; et al. Unveiling the proton-feeding effect in sulfur-doped Fe-N-C single-atom catalyst for enhanced CO_2 electroreduction. *Angew. Chem. Int. Ed.* **2022**, *61*, e202206233. DOI
93. Wen, M.; Sun, N.; Jiao, L.; Zang, S. Q.; Jiang, H. L. Microwave-assisted rapid synthesis of MOF-based single-atom Ni catalyst for CO_2 electroreduction at ampere-level current. *Angew. Chem.* **2024**, *63*, e202318338. DOI PubMed
94. Fan, B.; Wang, W.; Liu, Z.; Guo, J.; Yuan, H.; Tan, Y. Recent progress in single atomic catalysts for electrochemical N_2 fixation. *Microstructures* **2024**, *4*, 2024025. DOI
95. Wang, Q.; Lei, Y.; Wang, D.; Li, Y. Defect engineering in earth-abundant electrocatalysts for CO_2 and N_2 reduction. *Energy. Environ. Sci.* **2019**, *12*, 1730-50. DOI
96. Zhang, R.; Jiao, L.; Yang, W.; Wan, G.; Jiang, H. Single-atom catalysts templated by metal-organic frameworks for electrochemical nitrogen reduction. *J. Mater. Chem. A.* **2019**, *7*, 26371-7. DOI
97. Wu, Z. Y.; Karamad, M.; Yong, X.; et al. Electrochemical ammonia synthesis via nitrate reduction on Fe single atom catalyst. *Nat. Commun.* **2021**, *12*, 2870. DOI PubMed PMC

98. Langevelde PH, Katsounaros I, Koper MT. Electrocatalytic nitrate reduction for sustainable ammonia production. *Joule* **2021**, *5*, 290-4. DOI
99. Sathishkumar, N.; Wu, S.; Chen, H. Mechanistic exploring the catalytic activity of single-atom catalysts anchored in graphitic carbon nitride toward electroreduction of nitrate-to-ammonia. *Appl. Surf. Sci.* **2022**, *598*, 153829. DOI
100. Zhang, S.; Jin, M.; Shi, T.; et al. Electrocatalytically active Fe-$(O\text{-}C_2)_4$ single-atom sites for efficient reduction of nitrogen to ammonia. *Angew. Chem. Int. Ed.* **2020**, *59*, 13423-9. DOI
101. Xu, J.; Zhang, S.; Liu, H.; et al. Breaking local charge symmetry of iron single atoms for efficient electrocatalytic nitrate reduction to ammonia. *Angew. Chem. Int. Ed.* **2023**, *62*, e202308044. DOI